Available on the CERN CDS information server

CMS PAS SUS-13-019

CMS Physics Analysis Summary

Contact: cms-pag-conveners-susy@cern.ch

2014/02/04

Search for supersymmetry in hadronic final states using M_{T2} with the CMS detector at $\sqrt{s} = 8$ TeV

The CMS Collaboration

Abstract

A search for supersymmetry or similar new physics is carried out using a sample with 19.5 fb^{-1} integrated luminosity of $\sqrt{s} = 8$ TeV pp collisions collected by the CMS experiment at the LHC. Our main approach, the inclusive M_{T2} analysis, is based on fully hadronic final states. Events are selected using the stransverse mass variable, M_{T2}, and analyzed separately for different jet and b-tagged jet multiplicities. The signal is separated from the standard model background by requiring high values of M_{T2}. The remaining backgrounds consist of Z+jets events where the Z decays to neutrinos, W+jets events, and $t\bar{t}$+jets events, where one W is decaying leptonically, but the charged lepton escaping detection. A second line of approach, the M_{T2} Higgs analysis, targets supersymmetric models with a Higgs boson produced within supersymmetric cascades and exploits the dominant decay channel to $b\bar{b}$. We search for a signal in the invariant mass distribution of the selected b pairs. For both approaches, all backgrounds are estimated using data-driven methods. No significant excess of events over the expected background is observed. Exclusion limits in various simplified models are derived.

1 Introduction

This document describes a search for physics beyond the standard model (SM) in pp collisions collected by the Compact Muon Solenoid (CMS) experiment at the Large Hadron Collider (LHC) at a centre-of-mass energy of 8 TeV. The results are based on the data sample collected in 2012, amounting to 19.5 fb^{-1} of integrated luminosity.

It is well known that a fully hadronic final state accompanied by a large missing transverse momentum ($E_{\mathrm{T}}^{\mathrm{miss}}$) is very sensitive to a broad class of new physics models, including supersymmetry (SUSY) [1] with R-parity conservation. We present results on the search for supersymmetry with R-parity conservation in hadronic final states using M_{T2}, the stransverse mass variable [2]. The variable M_{T2} is the natural extension of the classical transverse mass M_{T} in case of two pair-produced heavy particles, each decaying into several detectable and at least one undetected particle. For example, in supersymmetry two sparticles are pair-produced and both decay through a cascade of jets and leptons to the lightest supersymmetric particle (LSP). The LSP is not visible in the detector and leads to signature with large amount of $E_{\mathrm{T}}^{\mathrm{miss}}$. Though M_{T2} was originally introduced to derive the masses of sparticles involved in the cascade decay, we use it here purely as discovery variable, since it is very sensitive to the presence of new SUSY-like physics. Indeed, the distribution of M_{T2} reflects the produced particle masses and these are much lighter for the SM background processes than for the SUSY processes we are looking for. Hence, new physics is expected to show up as an excess in the tail of M_{T2}. The calculation of M_{T2} is based on clustering jets together to form two systems, called pseudo-jets.

The variable M_{T2} has previously been used for top mass measurements in the dileptonic final state by the CDF collaboration [3], and for SUSY searches by the ATLAS [4, 5] and CMS [6] collaborations in dileptonic and hadronic final states, respectively.

The inclusive M_{T2} analysis aims at covering a large variety of possible signals of beyond the standard model (BSM) physics. This is achieved by using a multi-bin approach. We divide the topologies of events into several regions defined by the number of jets (N_j) and the number of b jets (N_b), where a b jet is a jet originating from a b-quark hadronization. In addition to the topologies, the events are also subdivided in several kinematic regions. Three bins are used for the H_{T}, defined as the scalar sum of the jet transverse momenta, and up to nine bins in M_{T2}. With this approach, we target, in case of SUSY, events resulting from heavy sparticle production, characterized by large $E_{\mathrm{T}}^{\mathrm{miss}}$ and large M_{T2}.

We design a set of selection criteria that enhances a potential SUSY signal and removes instrumental and multijet backgrounds containing fake $E_{\mathrm{T}}^{\mathrm{miss}}$ due to mismeasurements. We show with simulation that the remaining SM backgrounds in the signal region consist mainly of $W(l\nu)$+jets, $Z(\nu\bar{\nu})$+jets and semileptonic $t\bar{t}$ production, which are estimated by data-driven methods.

As an extension of the inclusive M_{T2} analysis, events with at least two b jets are used to look for the possible decay of SUSY cascades into the light Higgs boson, itself decaying into its dominant channel $b\bar{b}$. This analysis is called M_{T2} Higgs analysis. The boson that has been observed around $M_h \sim 125\,\text{GeV}$, can be the lightest Higgs boson (h^0) within the framework of the minimal supersymmetric extension of the standard model (MSSM). A dedicated selection is applied and the search is performed using the invariant mass of the two b jets.

We observe good agreement between the data and the data-driven prediction within the uncertainties and find no evidence for a new physics signal. We derive exclusion limits on the signal cross section times branching ratio within our acceptance. We also estimate the 95% C.L. exclusions for several simplified model scans (SMS) [7].

A result was published based on data corresponding to 5 fb^{-1} at a centre-of-mass energy of 7 TeV in [6]. The present document is a continuation and development of that analysis using the full 2012 data set, and extends previous results in fully hadronic final states at $\sqrt{s} = 8\,\mathrm{TeV}$ by the ATLAS [8, 9] and CMS [10, 11] collaborations.

This note is organized as follows: after a brief introduction to M_{T2} and its salient properties in Section 2, and a summary of the CMS detector in Section 3, we describe in Section 4 the data samples used and the event selection. In Section 5, the search strategy is presented and applied to the inclusive M_{T2} analysis in Section 6 and to the M_{T2} Higgs analysis in Section 7. In these sections, the data-driven background estimations are discussed. The results are presented in Section 8. We proceed with establishing exclusion limits in Section 10. Finally, Section 11 contains our conclusions.

2 Definition of M_{T2} and interpretation

The properties of M_{T2} were discussed in the previous publication [6]. Here, we recapitulate the most important features. The variable M_{T2} or stranverse mass was introduced [2] to measure the mass of primary pair-produced particles in a situation where both ultimately decay into undetected particles (like neutralino LSPs) leaving the event kinematics underconstrained. It assumes that the two produced sparticles give rise to identical types of decay chains with two visible systems defined by their transverse momenta, $\vec{p}_{\mathrm{T}}^{\,\mathrm{vis}(i)}$, energies $E_{\mathrm{T}}^{\mathrm{vis}(i)}$, and masses $m^{\mathrm{vis}(i)}$. They are accompanied by the unknown LSP transverse momenta, $\vec{p}_{\mathrm{T}}^{\,\tilde{\chi}(i)}$. In analogy with the transverse mass used for the W mass determination, we can define two transverse masses ($i = 1, 2$)

$$(M_{\mathrm{T}}^{(i)})^2 = (m^{\mathrm{vis}(i)})^2 + m_{\tilde{\chi}}^2 + 2\left(E_{\mathrm{T}}^{\mathrm{vis}(i)} E_{\mathrm{T}}^{\tilde{\chi}(i)} - \vec{p}_{\mathrm{T}}^{\,\mathrm{vis}(i)} \cdot \vec{p}_{\mathrm{T}}^{\,\tilde{\chi}(i)}\right). \tag{1}$$

These have the property (like for W boson decay) that for the true LSP mass their distribution cannot exceed the mass of the parent particle of the decay and they present an endpoint at the value of the parent mass. The momenta $\vec{p}_{\mathrm{T}}^{\,\tilde{\chi}(i)}$ of the unseen particles are not experimentally accessible individually and only their sum, the vector of the missing transverse momentum $\vec{p}_{\mathrm{T}}^{\,\mathrm{miss}}$, is known. Therefore, in the context of SUSY, a generalization of the transverse mass is needed and the proposed variable is M_{T2}. It is defined as

$$M_{\mathrm{T2}}(m_{\tilde{\chi}}) = \min_{\vec{p}_{\mathrm{T}}^{\,\tilde{\chi}(1)} + \vec{p}_{\mathrm{T}}^{\,\tilde{\chi}(2)} = \vec{p}_{\mathrm{T}}^{\,\mathrm{miss}}} \left[\max\left(M_{\mathrm{T}}^{(1)}, M_{\mathrm{T}}^{(2)}\right)\right], \tag{2}$$

where the LSP mass $m_{\tilde{\chi}}$ remains as a free parameter. This formula can be understood as follows. As neither $M_{\mathrm{T}}^{(1)}$ nor $M_{\mathrm{T}}^{(2)}$ can exceed the parent mass if the true momenta are used, the larger of the two can be chosen. To make sure that M_{T2} does not exceed the parent mass, a minimization is performed on trial LSP momenta fulfilling the $E_{\mathrm{T}}^{\mathrm{miss}}$ constraint. The distribution of M_{T2} for the correct value of $m_{\tilde{\chi}}$ then has an endpoint at the value of the primary particle mass. If, however, $m_{\tilde{\chi}}$ is lower (higher) than the correct mass value, the endpoint will be below (above) the parent mass. In this document, we use M_{T2} as a variable to distinguish SUSY production events from SM backgrounds, after having clustered the jets to form two pseudo-jets. The computation of M_{T2} is done using the code of [12].

A method to subdivide multijet events into two pseudo-jets is the reconstruction of "event hemispheres" described in [13], Section 13.4. The hemisphere reconstruction works as follows: first, two initial axes (seeds) are chosen. Here, we take them as the directions of the two massless jets that have the largest dijet invariant mass. Next, the other jets are associated to one of these axes according to a clustering criterion (hemisphere association method). We used the minimal Lund distance [14], meaning that jet k is associated to the hemisphere i rather than j if:

$$(E_i - p_i \cos\theta_{ik}) \frac{E_i}{(E_i + E_k)^2} \leq (E_j - p_j \cos\theta_{jk}) \frac{E_j}{(E_j + E_k)^2}, \tag{3}$$

where E_k and p_k are the energy and momentum of jet k and θ_{jk} is the polar angle between jet k and hemisphere j. After all jets are associated to one or the other axis, the axes are recalculated as the sum of the momenta of all jets connected to a hemisphere and the association is iterated using these new axes until no jet switches from one group to the other.

Because of the large mass scale of produced sparticles, SUSY events with large expected $E_{\mathrm{T}}^{\mathrm{miss}}$ and large jet acoplanarity will be concentrated in the large M_{T2} region. On the contrary, mismeasured dijet events, being back-to-back, will populate the region of minimum M_{T2}, regardless of the magnitude of the $E_{\mathrm{T}}^{\mathrm{miss}}$ or jet p_{T}. Hence, M_{T2} has a built-in protection against jet mismeasurements, even if they have a large $E_{\mathrm{T}}^{\mathrm{miss}}$. However, mismeasured multijet events may give rise to pseudo-jets away from the back-to-back configuration, leading to non-zero M_{T2}. For this reason, further protections against $E_{\mathrm{T}}^{\mathrm{miss}}$ from mismeasurements are introduced. Multijet events, interpreted as two massive pseudo-jets, may give rise to large M_{T2}, even though the pseudo-jets are back-to-back, in case that both pseudo-jets have high masses. Therefore, defining pseudo-jets as massless is a good approach towards further suppressing multijet events in the M_{T2} tail while maintaining good signal sensitivity. Other backgrounds consist of events containing true $E_{\mathrm{T}}^{\mathrm{miss}}$, as these can lead to pseudo-jets away from the back-to-back configuration. Candidates are top ($t\bar{t}$+jets and single top), $W(l\nu)$+jets with leptonic decays and $Z(\nu\bar{\nu})$+jets production. In the following, M_{T2} is computed for massless pseudo-jets and $m_{\tilde{\chi}} = 0$.

3 CMS detector

The central feature of the CMS apparatus is a superconducting solenoid, 13 m in length and 6 m in diameter, that provides an axial magnetic field of 3.8 T. The core of the solenoid is instrumented with various particle detection systems: a silicon pixel and strip tracker, an electromagnetic calorimeter (ECAL), and a brass/scintillator hadron calorimeter (HCAL). The silicon pixel and strip tracker covers $|\eta| < 2.5$, where pseudorapidity η is defined by $\eta = -\ln\tan(\theta/2)$ with θ the polar angle of the trajectory of the particle with respect to the counterclockwise beam direction. The ECAL and HCAL cover $|\eta| < 3$. The steel return yoke outside the solenoid is instrumented with gas detectors used to identify muons. A quartz-steel Cerenkov-radiation-based forward hadron calorimeter extends the coverage to $|\eta| \leq 5$. The detector is nearly hermetic, covering $0 < \phi < 2\pi$ in azimuth, allowing for energy balance measurements in the plane transverse to the beam directions. The first level of the CMS trigger system, composed of custom hardware processors, uses information from the calorimeters and muon detectors to select the most interesting events in a fixed time interval of less than 4 μs. The High Level Trigger processor farm further decreases the event rate from around 100 kHz to around 300 Hz, before data storage. A detailed description of the CMS detector can be found elsewhere [15].

4 Datasets and event selection

The analysis strategy is designed using Monte Carlo simulation (MC). The simulated SM samples are generated with MADGRAPH 5 [16], PYTHIA 6.4 [14] and Powheg [17]. Simulated signal samples are produced with MADGRAPH 5 using the CTEQ6L1 [18] parton distribution functions; up to two additional partons are present in the matrix element calculations. PYTHIA

6.4 is used for the parton shower and hadronization simulation. All simulated samples are processed with a detailed simulation of the CMS detector response based on GEANT4 [19]. The simulated events are reconstructed and analyzed in the same way as the data. In the case of SM background simulation samples we have used the most accurate calculation of the cross sections available in the literature, usually at next-to-leading order (NLO). For the SUSY SMS signal samples we used NLO cross sections calculated with Prospino [20] and [21–25].

The events are reconstructed using the particle-flow (PF) algorithm [26], which identifies and reconstructs individually the particles produced in the collision, namely charged hadrons, photons, neutral hadrons, muons, electrons and taus.

Electrons and muons with a transverse momentum of $p_{\mathrm{T}} \geq 10\,\mathrm{GeV}$ and $|\eta| \leq 2.4$ are considered isolated, if the transverse momentum sum of charged hadrons, photons, and neutral hadrons surrounding the lepton, with $\Delta R = \sqrt{\Delta\eta^2 + \Delta\phi^2} < 0.3$, divided by the lepton transverse momentum itself was less than 0.15 and 0.2, respectively, after correcting for the effect of pileup, namely multiple pp collisions within a beam crossing. The electron and muon reconstruction and identification are described in [27] and [28], respectively. All particles apart from the isolated electrons and muons are then clustered into jets by the anti-k_{T} jet clustering algorithm [29] with a distance parameter $R = 0.5$ forming PF jets [30, 31]. Jet energies are calibrated by applying correction factors as a function of the transverse momentum and the pseudorapidity of the jet. Residual jet energy corrections are applied in order to match the jet energy scales in data and simulation [32]. The effect of pileup on jet energies are treated as follows: tracks, which are not coming from the primary interaction are removed, while for the neutral part the effect of pileup is reduced by using the FastJet pileup subtraction procedure [33, 34] for data and simulation. Jets are required to pass loose quality requirements on the hadronic, electromagnetic, as well as neutral and charged energy fractions (jet ID), satisfy $p_{\mathrm{T}} \geq 40\,\mathrm{GeV}$, and be within $|\eta| \leq 2.4$. Jets are identified as originating from b-quark hadronization by the combined secondary vertex (CSV) algorithm with a medium working point [35]. These jets are called b jets. Tau leptons that decay hadronically into one or three charged particles plus several or none neutral particles are considered if they have $p_{\mathrm{T}} \geq 20\,\mathrm{GeV}$ and $|\eta| \leq 2.3$. They further need to satisfy a loose isolation criterium: the transverse momentum sum of charged hadrons and photons within $\Delta R < 0.5$ to the tau candidate is required to be less than 2 GeV, after being corrected for the effect of pileup. Hereafter, tau leptons decaying hadronically will be simply referred to as taus. Photons are considered if $p_{\mathrm{T}} \geq 20\,\mathrm{GeV}$ and $|\eta| \leq 2.4$ excluding the transition region between barrel and endcap ($1.442 < |\eta| < 1.566$). They are required to satisfy shower shape criteria, leave little deposit in the hadron calorimeter and fulfill isolation requirements.

The data used in this analysis are collected by triggers based on the scalar sum of transverse momenta of reconstructed and energy corrected PF jets with $p_{\mathrm{T}} \geq 40\,\mathrm{GeV}$ (H_{T}), and/or on $E_{\mathrm{T}}^{\mathrm{miss}}$, computed as the absolute value of the vector sum of all particles reconstructed by the PF algorithm. Three sets of triggers are used: a H_{T} trigger select events that satisfy $H_{\mathrm{T}} \geq 650\,\mathrm{GeV}$ online. The logical OR of an $E_{\mathrm{T}}^{\mathrm{miss}}$ trigger with an online threshold of 150 GeV, and a H_{T}-$E_{\mathrm{T}}^{\mathrm{miss}}$ trigger with online thresholds of $H_{\mathrm{T}} \geq 350\,\mathrm{GeV}$ and $E_{\mathrm{T}}^{\mathrm{miss}} \geq 100\,\mathrm{GeV}$ are used to efficiently select events with lower H_{T}.

Events are required to have at least one well reconstructed primary vertex [36]. The triggers are measured to be $> 99\%$ efficient in the region where events are selected offline with $H_{\mathrm{T}} > 750\,\mathrm{GeV}$ for the H_{T} triggers, and with $H_{\mathrm{T}} > 450\,\mathrm{GeV}$ and $E_{\mathrm{T}}^{\mathrm{miss}} > 200\,\mathrm{GeV}$ for the $E_{\mathrm{T}}^{\mathrm{miss}}$-based triggers. At least two good jets are required, the two leading jets with $p_{\mathrm{T}} \geq 100\,\mathrm{GeV}$. Events with possible contributions from beam halo processes, anomalous calorimeter or tracking noise are rejected. In order to reject events with an important contribution of soft and/or forward jets to the momentum imbalance, a maximum difference of 70 GeV is imposed between the $E_{\mathrm{T}}^{\mathrm{miss}}$ vector and the vector sum of the p_{T} of all leptons and jets candidates with $p_{\mathrm{T}} > 20\,\mathrm{GeV}$ passing the jet ID. An event is also rejected if it contains hard jet candidates failing the jet ID.

It has been argued previously that M_{T2} is protected against jet energy mismeasurements in dijet events. In multijet events such mismeasurement can lead to hemispheres not being back-to-back and resulting in larger values of M_{T2}. To protect against this effect, a minimum difference in azimuth ϕ between any of the four leading jets and the $E_{\mathrm{T}}^{\mathrm{miss}}$, $\Delta\phi_{\mathrm{min}} \geq 0.3$, is required. Finally, events are vetoed if they contain an isolated electron, muon or tau, to suppress the contributions from $W(l\nu)$+jets, $Z(ll)$+jets, and top backgrounds.

5 Search strategy

We will now outline the strategy of the M_{T2}-based analysis. We cluster all jet candidates ($p_{\mathrm{T}} > 20\,\mathrm{GeV}$, $|\eta| < 2.4$, loose jet ID) into two pseudo-jets using the algorithm of Section 2. Massless pseudo-jets have been used as input to M_{T2} and zero test mass, as this was found to be the most efficient way of reducing the multijet background. We subdivided the analysis in several mutually exclusive regions to optimize the search to a large variety of possible BSM physics models. The signal regions are based on either the event topology or the kinematics, the search strategy is developed as follows:

1. Topological regions are defined by N_j and N_b in the event, as illustrated in Fig. 1 (left), amounting to nine different regions. The choice of these regions has been deduced from simulation by testing the sensitivity to various models of BSM physics. In the case of SUSY, the 0 b-jet bins are most sensitive to the production of squarks of the first two generations and gluinos. The b-enriched signal regions with low jet multiplicity are aimed at stop and sbottom production with decays to b jets while the high jet multiplicity regions are more sensitive to stop and sbottom production with decays to top quarks. Finally, the signal regions with $N_j \geq 3$ and $N_b \geq 3$ provide extra sensitivity to final states with multiple bottom or top quarks, like from gluino pair production.

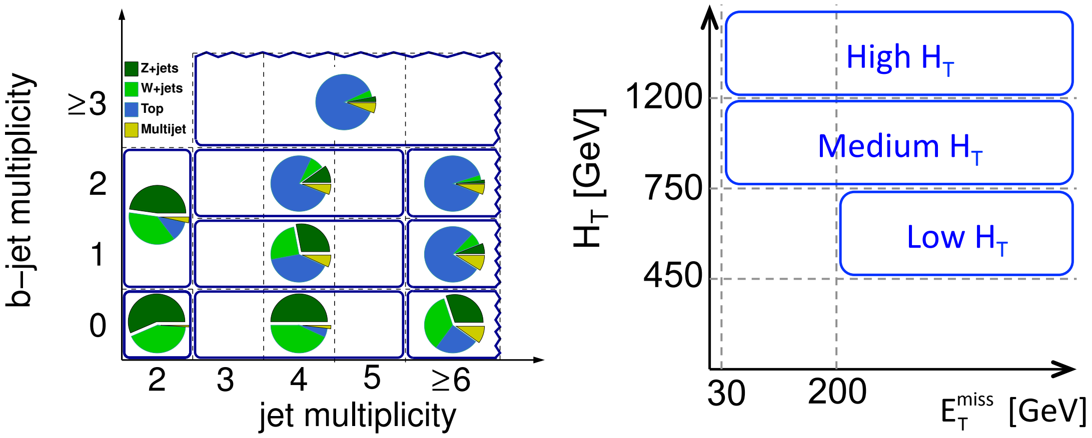

Figure 1: (left) Definition of the topological regions in number of jets and number of b jets. The pie charts show the relative expected contribution from different SM backgrounds to the signal regions for each topological region. (right) Binning in H_{T} and $E_{\mathrm{T}}^{\mathrm{miss}}$.

2. The size of M_{T2} and H_{T} in a SUSY event is dependent on the sparticle mass and therefore

a wide range in M_{T2} and H_T is considered. Three regions are defined in H_T, the low H_T region for $450 \leq H_T < 750\,\text{GeV}$, the medium H_T region for $750 \leq H_T < 1200\,\text{GeV}$ and the high H_T region extending above 1200 GeV in H_T, shown in Fig. 1 (right). The lowest threshold in H_T is determined by the trigger requirements. For the low H_T region a minimum E_T^{miss} of 200 GeV is required because of the trigger selection.

3. In each of these regions, several adjacent bins in M_{T2} are defined (up to nine) with the number of bins depending on the H_T and topological regions. The lowest bin in M_{T2} is chosen such that the multijet background is expected to be less than $\sim 1 - 10\%$ of the total background. For the low H_T region the lowest requirement in M_{T2} is set to 200 GeV, as below 200 GeV the M_{T2} distribution is distorted by the E_T^{miss} requirement. The other bins are adjusted to have a sufficient number of events remaining (from SM) in each, to allow for an estimate of the different background contributions. The exact binning is found in Table 1.

4. Data-driven methods are designed for each of the different background contributions. The numbers of events and their systematic uncertainties are computed by means of these methods in each topological region and bin of H_T and M_{T2}. The background prediction methods are described in Sections 6.1-6.3.

5. The predicted numbers of events for all background components and their uncertainties are summed bin by bin, giving an estimate of the total background in each bin. The estimated number of background events for each bin are compared to the number of observed events.

6. The potential contribution from a SUSY signal is quantified by a statistical method based on a multi-bin profile likelihood described in Section 9.

7. In addition to the inclusive M_{T2} search discussed above, aiming for general SUSY signatures in hadronic final states, there is a search targeted for Higgs boson production within SUSY cascades, the M_{T2} Higgs analysis, which shares signal regions and background estimation methods with the inclusive M_{T2} search but is optimized for the lightest MSSM Higgs boson. The Higgs boson signal is searched in its main decay mode to $b\bar{b}$.

After the event selection, we do not expect a significant amount of multijet events to enter the signal regions. Nevertheless, we use a data-driven method to estimate the amount of remaining multijet background in the signal regions. We will demonstrate in the following sections that the background mainly consists of production of electroweak bosons ($W(l\nu)$+jets and $Z(\nu\bar{\nu})$+jets) and production of top quark pairs ($t\bar{t}$+jets). Those events contain real E_T^{miss} due to the presence of at least one neutrino. All backgrounds are predicted by the means of data-driven methods.

The results will be interpreted in terms of several simplified models.

6 The inclusive M_{T2} analysis

Figure 2 shows the M_{T2} distributions from simulation and data for low, medium, and high H_T, inclusively in all bins of the $N_j - N_b$ plane.

For $M_{T2} < 80$ GeV the distribution in the medium and high H_T region is completely dominated by multijet events. Therefore, the low M_{T2} regions are not part of any signal region: the lowest M_{T2} bins start from $100 - 200\,\text{GeV}$, depending on the topological and H_T region. In the lowest

Table 1: Signal bin definitions of the inclusive M_{T2} analysis.

	low H_T region			medium H_T region			high H_T region	
	M_{T2} bin [GeV]			M_{T2} bin [GeV]			M_{T2} bin [GeV]	
2 jets, 0 b jets	200-240 240-290 290-350	350-420 420-490 490-570	570-650 ≥ 650	125-150 150-180 180-220	220-270 270-325 325-425	425-580 580-780 ≥ 780	120-150 150-200 200-260	260-350 350-550 ≥ 550
2 jets, ≥ 1 b jets	200-250 250-310	310-380 380-450	450-550 ≥ 550	100-135 135-170	170-260 260-450	≥ 450	100-180 ≥ 180	
3-5 jets, 0 b jets	200-240 240-290 290-350 350-420	420-490 490-570 570-650 ≥ 650		160-185 185-215 215-250 250-300	300-370 370-480 480-640 640-800	≥ 800	160-185 185-220 220-270 270-350	350-450 450-650 ≥ 650
3-5 jets, 1 b jets	200-250 250-310	310-380 380-450	450-550 ≥ 550	150-175 175-210	210-270 270-380	380-600 ≥ 600	150-180 180-230	230-350 ≥ 350
3-5 jets, 2 b jets	200-250 250-325	325-425 ≥ 425		130-160 160-200	200-270 270-370	≥ 370	130-200 ≥ 200	
≥ 6 jets, 0 b jets	200-280 280-380	≥ 380		160-200 200-250	250-325 325-425	≥ 425	160-200 200-300	≥ 300
≥ 6 jets, 1 b jets	200-250 250-325	≥ 325		150-190 190-250	250-350 ≥ 350		150-200 200-300	≥ 300
≥ 6 jets, 2 b jets	200-250 250-300	≥ 300		130-170 170-220	220-300 ≥ 300		120-200 ≥ 200	
≥ 3 jets, ≥ 3 b jets	200-280	≥ 280		125-175	175-275	≥ 275	1≥ 125	

M_{T2} bins of the signal region, a small contribution of order $\leq$ 10% from multijet events is expected.

In the signal regions with events containing exactly two jets or events with 0 b jets, the dominant background is $Z(\nu\bar{\nu})$+jets production, followed by leptonic $W(l\nu)$+jets production, with only a small contribution of $t\bar{t}$+ jets production. In the regions with 1 b jet all three processes ($Z(\nu\bar{\nu})$+jets, $W(l\nu)$+jets, and $t\bar{t}$+jets production) are important. For all regions having with multiple b jets, $t\bar{t}$+jets events are the dominant source of backgrounds. The $t\bar{t}$+jets component typically increases with higher jet multiplicity and is important for all selections with $N_j \geq 6$, regardless of the b-jet selection. In addition to the features described, the relative contribution of $t\bar{t}$+jets production decreases for higher M_{T2} by the virtue of the M_{T2} variable. Contributions from other backgrounds, such as γ+jets, $Z(ll)$+jets and diboson production, are found to be negligible. These observations apply to all three H_T regions.

6.1 Data-driven determination of the multijet background

From studies with simulation, we have determined that the multijet background is negligible in the tail of the M_{T2} distribution. Nevertheless, a data-driven method is designed to verify that this is indeed the case.

We use a method based on M_{T2} and $\Delta\phi_{\min}$. The background in the signal region, defined by $\Delta\phi_{\min} \geq 0.3$ and large M_{T2}, is predicted from a control region with $\Delta\phi_{\min} \leq 0.2$. The two variables are strongly correlated, but a factorization method is applied since the functional

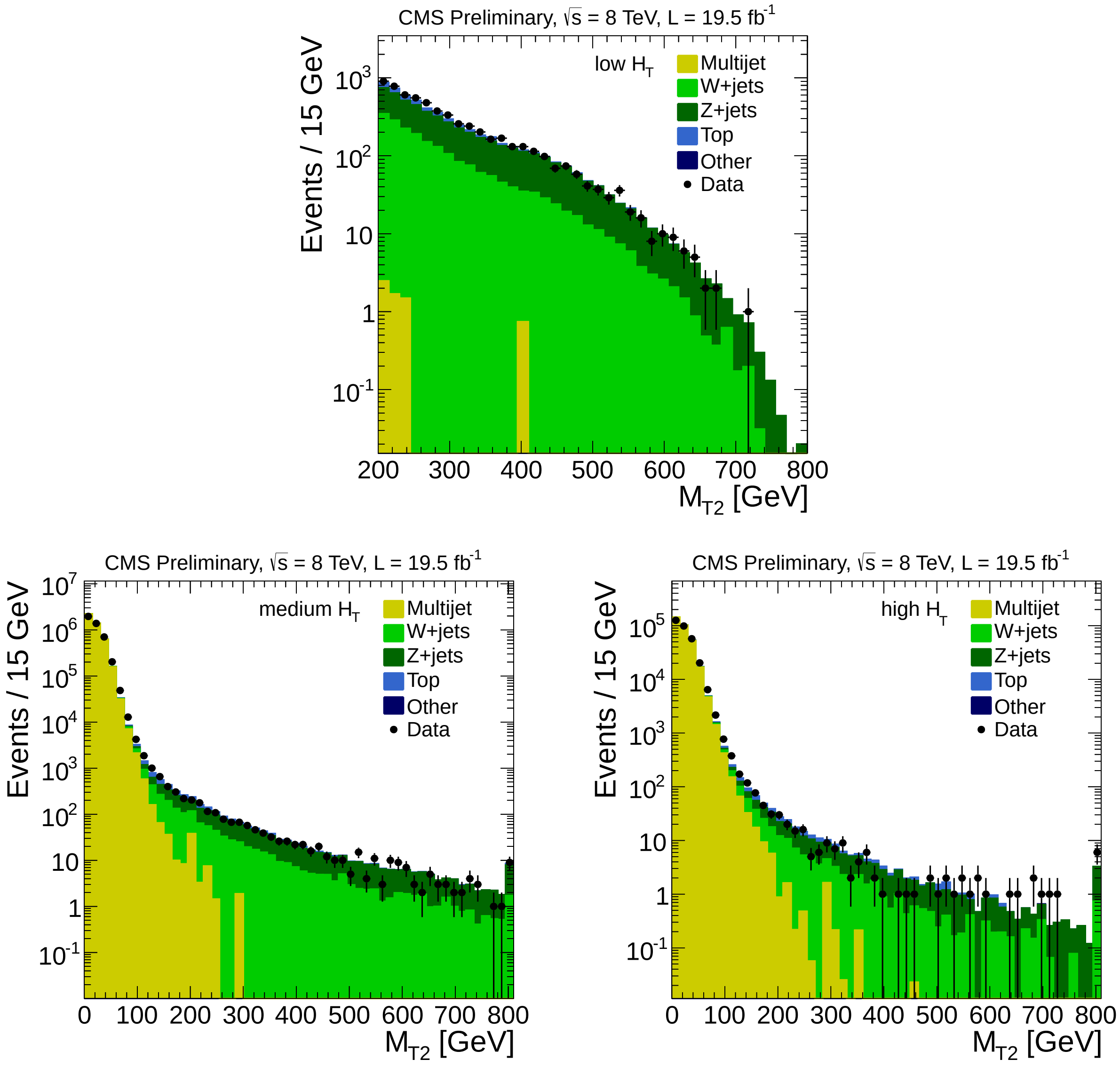

Figure 2: M_{T2} for massless pseudo-jets after full selection for the low H_T (top), medium H_T (bottom left) and high H_T region (bottom right), summed over all regions in the (N_j, N_b) plane, for simulation and data. The data correspond to an integrated luminosity of 19.5 fb^{-1}. The last bins contain the overflow. The different simulated backgrounds are stacked on top of each other and normalized to the integrated luminosity.

form is known for the ratio of numbers of events $r(M_{T2}) = N(\Delta\phi_{\min} \geq 0.3)/N(\Delta\phi_{\min} \leq 0.2)$ as a function of M_{T2}. It is found in studies with simulation, and confirmed in data, that for $M_{T2} > 50\,\text{GeV}$ the ratio falls off exponentially and, therefore, a parameterization of the form

$$r(M_{T2}) = \frac{N(\Delta\phi_{\min} \geq 0.3)}{N(\Delta\phi_{\min} \leq 0.2)} = \exp(a - b \cdot M_{T2}) + c \tag{4}$$

is used for $M_{T2} > 50\,\text{GeV}$. The function is assumed to reach a constant value at large M_{T2} due to extreme tails of the jet energy resolution. We check in simulated multijet events that correct results are obtained when the fit is limited to the region $50 < M_{T2} < 80\,\text{GeV}$, where the contribution of electroweak and top (mainly $t\bar{t}$+jets) processes is small. The constant term, however, is only measurable in the signal region when using simulation event samples. First, a validation test is performed by estimating the multijet contamination using the predicted events in multijet simulation samples, applying the parameterization model above. A good agreement is observed. The robustness of the prediction is further checked by varying the fit boundaries and the cut value on $\Delta\phi_{\text{min}}$. Next, the exponential part of Eq. (4) is fitted to data to extract parameters a and b. For this we use the data in the region $50 < M_{\text{T2}} < 80\,\text{GeV}$ after subtracting the electroweak and top ($t\bar{t}$+jets and single top production) contribution. An example of the fit is shown in Fig. 3. The parameter c is fixed conservatively to the value of the exponential fit at $M_{\text{T2}} = 200\,\text{GeV}$ where the agreement of the exponential with data can still be tested.

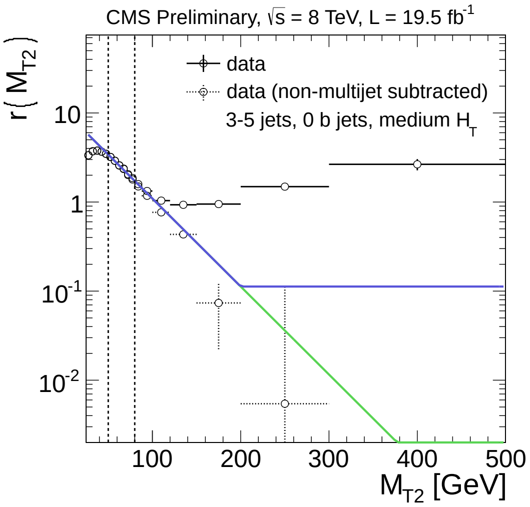

Figure 3: Value of $r(M_{\text{T2}})$ versus M_{T2} for the data events with the fit superposed. A wide M_{T2} range is shown for the medium H_{T} selection and the region of 3-5 jets and 0 b jets. The points with solid uncertainty bars correspond to raw data after all selection cuts, while the points with dashed uncertainty bars correspond to data after subtracting $W(l\nu)$+jets, $Z(\nu\bar{\nu})$+jets and $t\bar{t}$+jets backgrounds. A fit to an exponential (green curve) is performed in the region $50 < M_{\text{T2}} < 80\,\text{GeV}$ where the non-multijet contribution is minimal. The constant term of the final functional parameterization (blue curve) is taken as the value of the exponential at $M_{\text{T2}} = 200\,\text{GeV}$. The fits well describe the data after subtracting the non-multijet background, even far away from the fit region.

In the low H_{T} region $E_{\text{T}}^{\text{miss}}$ triggers are used that distort distributions in the low M_{T2} region. Therefore, that data cannot be used to predict the multijet contribution. However, existing prescaled triggers, that are triggers that randomly select only a certain fraction of events passing the trigger selection, are used to access the low H_{T} region without any $E_{\text{T}}^{\text{miss}}$ requirement. Thus, we can extract the fit parameters from the low M_{T2} region.

In the lower M_{T2} bins, where the exponential term dominates over the constant term, the multijet prediction from data gives an accurate estimate. For the high M_{T2} bins the constant term dominates. It is important to note that the conservative overestimate of the multijet background for large M_{T2} with respect to simulation does not lead to a total background overprediction, since the final multijet background prediction is still negligible compared to the total background in the tail.

6.2 Data-driven determination of the $W(l\nu)$+jets and top background

The background due to W+jets production and top production (mainly $t\bar{t}$+jets, but also single top production) in the fully hadronic events has the following sources in common:

- leptonic decays of W, where the charged lepton is unobserved because of the acceptance cuts,
- leptonic decays of W, where the charged lepton is within the acceptance, but fails to satisfy the reconstruction, identification or isolation criteria.

For both sources, called lost lepton hereafter, we expect a slightly higher contribution from taus than for electrons or muons since the reconstruction efficiency for taus is smaller and the acceptance cuts are more stringent. In the following, we estimate the lost-lepton contribution in a data-driven way with all selection cuts applied but inverted lepton veto.

For the estimate of lost leptons, events with exactly one lepton in our various signal regions are used. The number of events containing one lepton is then scaled by a factor reflecting the probability to lose the lepton using the lepton efficiency and lepton acceptance that are taken from simulation. To protect against a potential contamination from signal events, a transverse mass cut $M_T < 100\,\text{GeV}$ on the lepton-E_T^{miss} system is introduced. Therefore, the factor is defined as $R_{LL} = \frac{1-\varepsilon(l)}{\varepsilon(l)\cdot\varepsilon(M_T)}$, where $\varepsilon(l)$ is the combined lepton efficiency and acceptance, and $\varepsilon(M_T)$ is the acceptance of the M_T selection. The factor R_{LL} is dependent on the selected signal region.

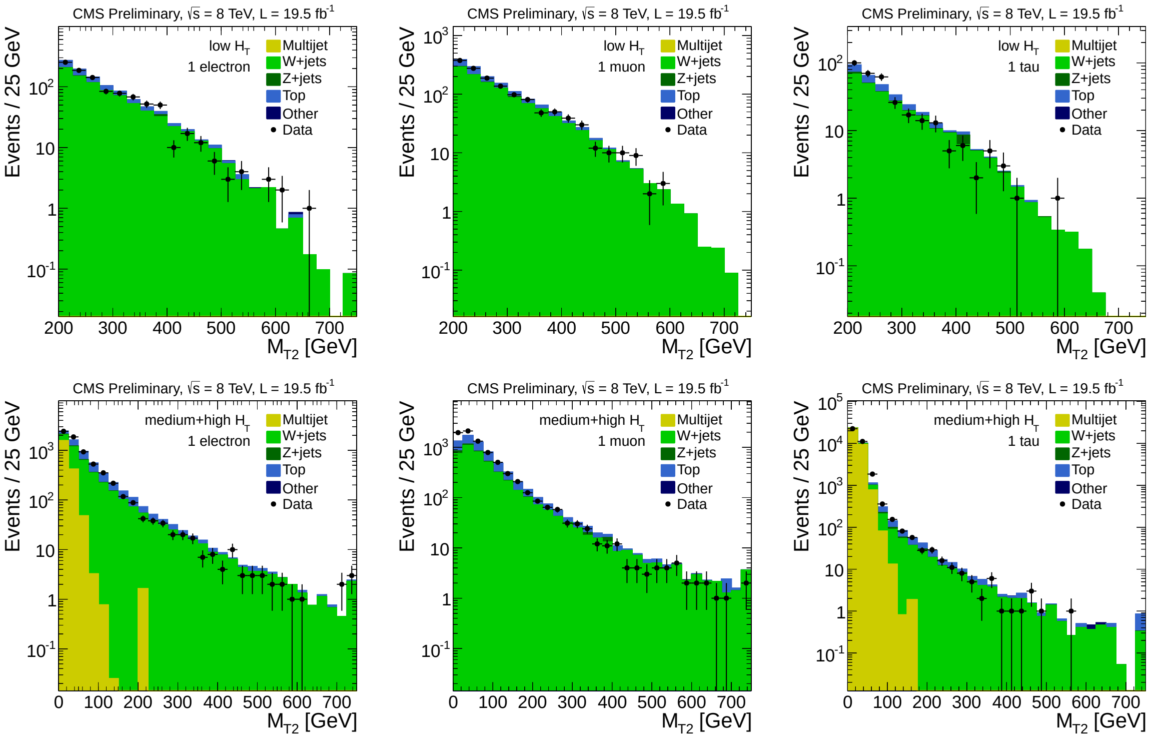

Figure 4: Distribution of M_{T2} for events with one electron (left), one muon (middle), or one tau (right) in data and simulation for the low H_T selection (upper plots) and for the medium and high H_T selection (bottom plots). The data correspond to an integrated luminosity of 19.5 fb^{-1}. All selection cuts are applied, but the lepton veto is inverted. We require $M_T < 100\,\text{GeV}$ on the lepton-E_T^{miss} system.

The M_{T2} distributions for events satisfying the full selection (as outlined in Section 4), but after requiring one reconstructed lepton are shown in Fig. 4 for data compared to the simulation, inclusively for all (N_j, N_b) signal regions. First, a successful validation test of the method is made using simulation. Then, the data-driven estimate is performed on the signal regions in the different H_T regions and all the (N_j, N_b) signal regions, but integrated over all M_{T2} bins. The shape along M_{T2} was obtained using simulation. As we expect a very small yield of events containing one lepton for large M_{T2}, the use of both data and simulation results in a more robust estimate of this background for large M_{T2}. The systematic uncertainty includes the uncertainty on the lepton efficiencies, acceptance and background subtraction and amounts to about 20%. In addition, the uncertainty of the simulated shape along M_{T2} is estimated by varying several parameters of the simulation, the important ones being the matching scale, the renormalization and factorization scales (using dedicated simulated samples), the jet energy scale [32], the b-tagging efficiency [35] and the p_T MC NLO uncertainty [37].

6.3 Data-driven determination of the $Z(\nu\bar{\nu})$+jets background

The estimate of the $Z(\nu\bar{\nu})$+jets background is obtained by selecting γ + jets and $Z(ll)$+jets events and the invisible decay of the Z boson is mimicked by removing the photon or the leptons from the event, and adding the corresponding p_T to the E_T^{miss} vector. All event variables, like M_{T2}, are subsequently recalculated.

As pointed out in [38], the Z+jets and γ+jets processes differ because of the different electroweak couplings and the non-zero Z boson mass. For vector boson transverse momenta much larger than m_Z, we expect the ratio of prompt-photon over Z production to be determined by the ratio of the respective couplings to quarks and thus to approach a constant value. Since the event kinematics (including the hadronic activity) are very similar at high boson p_T, γ+jets events are ideally suited to predict the $Z(\nu\bar{\nu})$+jets irreducible background in our signal region, as they provide reasonably large event yield. The estimation using only γ+jets events is not directly applicable for b-enriched events, as other processes contribute to this region.

The comparison between data and simulation of the M_{T2} distribution for the γ+jets events with no b jets is shown in Fig. 5. The photon p_T is added to the E_T^{miss} vector and all event variables are recalculated. In order to reduce the contamination of a potential signal to this event selection we require the true E_T^{miss}, before adding the reconstructed photon, to be less than 100 GeV. For the low H_T region, the events are selected by a single photon trigger, as we require the event to have low E_T^{miss}. For medium and high H_T our signal trigger can be used.

The photon selection contains both prompt photons as well as collinear photons from neutral pion decays within multijet events that are reconstructed as a single photon. The two components are disentangled by means of a maximum likelihood fit of simulation templates to the shower shape variable in data. The fit is performed separately in the ECAL barrel and endcaps for events without any M_{T2} requirement and no b jets. This event selection is dominated by low p_T photons, where the shower shape provides high discrimination power between prompt photons and photons from neutral pion decays. The extrapolation of their contributions as a function of M_{T2} was obtained from simulation by matching the overall purity of prompt photons to the one observed in data. The $Z(\nu\bar{\nu})$+jets background in the 0 b-jet events was estimated for each bin in M_{T2} from the number of prompt photon events multiplied by the M_{T2}-dependent ratio of $Z(\nu\bar{\nu})$+jets to γ+jets events obtained from simulation. This ratio increases as a function of the photon p_T (that drives the M_{T2} value) and reaches a constant value above 350 GeV, as seen from Fig. 6. The correctness of the simulation for the prediction of the distribution of the p_T of the Z boson is further checked by using events with a dileptonic decay

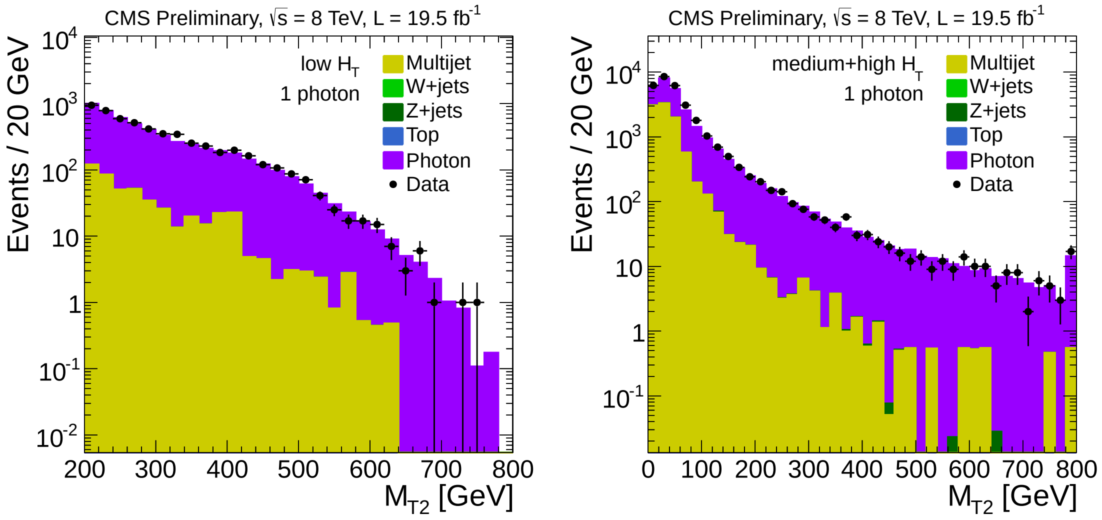

Figure 5: M_{T2} distributions for data and simulation after applying all selection cuts and requiring 0 b jets. The photon p_T is added to the E_T^{miss} vector and all event variables, including M_{T2}, are recalculated. Left: for the low H_T selection, Right: for the medium and high H_T selection. The data correspond to an integrated luminosity of 19.5 fb^{-1}.

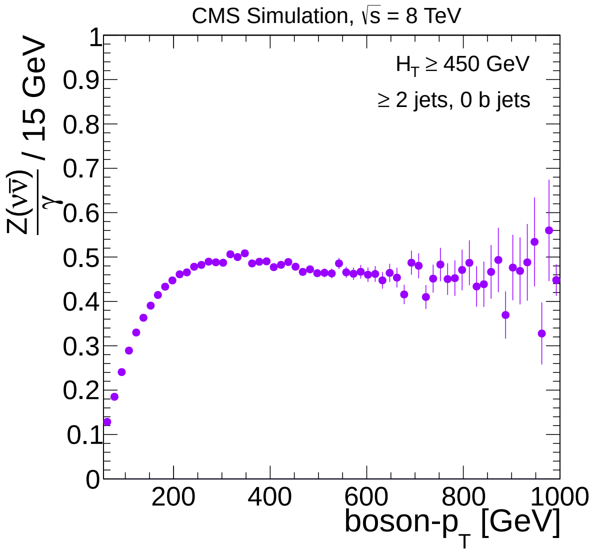

Figure 6: $Z(\nu\bar{\nu})/\gamma$ ratio from simulation as a function of the boson-p_T.

of the Z boson (that is $Z \to e^+e^-$ or $\mu^+\mu^-$) and is found to agree. The comparison between the dilepton events, selected by triggers requiring two leptons, and the simulation allows us to assign a systematic uncertainty of 20% to the $Z(\nu\bar{\nu})/\gamma$ ratio. For the bins of $M_{T2} > 350\,\text{GeV}$, this uncertainty is increased to 30% to allow for variations of the ratio in the tail of M_{T2}. The further uncertainties of the prediction methods are a normalization uncertainty in the shower shape fit of 5-10% for the medium and high H_T region, and 100% in the low H_T region due to the extrapolation in $p_T(\gamma)$, as well as the statistical uncertainties from the γ+jets event count.

As mentioned before, this estimate cannot directly be used for the b-enriched case, as other processes contribute to the b-enriched region. For the 1 b-jet case, the result from the 0 b jet are scaled by the ratio $Z_{ll}(1b)/Z_{ll}(0b)$ obtained from the dilepton data. The robustness of this ratio against the kinematic variables has been verified. For the events with multiple b jets, the $Z(\nu\bar{\nu})$+jets contribution is small compared to the other backgrounds and the simulation is used with an uncertainty of 100%. It has been checked in dileptonic events with $N_b \geq 2$ in the data that no excess over the estimate from simulation is observed, justifying the use of the simulation.

7 The M_{T2} Higgs analysis

This section presents a search for a light MSSM Higgs boson (h^0) produced in a cascade of supersymmetric particles starting with the strong production of squarks ($\tilde{q}$) and gluinos ($\tilde{g}$). Because of this production mechanism, the events can be efficiently triggered using the same triggers as in the inclusive M_{T2} analysis, and the dominant decay mode of the Higgs boson, $h^0 \to b\bar{b}$ can be exploited. The Higgs boson mass can be extracted from the reconstructed dijet mass distribution.

The main decay mode of the lightest MSSM Higgs boson (h^0) is the decay into a pair of bottom quarks ($b\bar{b}$). Without additional particles in the final state, events containing the $b\bar{b}$ topology cannot be triggered due to overwhelming multijet backgrounds. In case of production of h^0 in the decays of neutralinos (mainly $\tilde{\chi}_2^0 \to \tilde{\chi}_1^0 + h^0$), h^0 would be produced together with a neutralino $\tilde{\chi}_1^0$, therefore a minimum threshold on M_{T2} allows to exploit the $b\bar{b}$ configuration, because the multijet background is efficiently reduced. As the neutralino $\tilde{\chi}_2^0$ can be typical decay product of squarks and gluinos, the cross section can be very high [39, 40].

This analysis is defined complementary to the inclusive M_{T2} analysis. The final state is characterized by at least two b jets, significant $E_{\mathrm{T}}^{\mathrm{miss}}$, which is due to the production of the LSP, and multiple hard jets. In principle, the main background may come from supersymmetric processes themselves, for example b quarks are produced in sbottom quark decays. Also SM processes can produce multijet+$E_{\mathrm{T}}^{\mathrm{miss}}$ final states and contribute to the background: $t\bar{t}$+jets, $W(l\nu)$+jets and $Z(\nu\bar{\nu})$+jets production. Therefore, a search is based on a reduced phase-space with respect to the inclusive M_{T2} analysis:

- $N_j \geq 4$,
- $N_b \geq 2$, with $p_{\mathrm{T}} \geq 20\,\mathrm{GeV}$[1],
- $450 \leq H_{\mathrm{T}} < 750\,\mathrm{GeV}$, $E_{\mathrm{T}}^{\mathrm{miss}} > 200\,\mathrm{GeV}$, and $M_{\mathrm{T2}} > 200\,\mathrm{GeV}$ - called the low H_{T} region,
- $H_{\mathrm{T}} \geq 750\,\mathrm{GeV}$, $E_{\mathrm{T}}^{\mathrm{miss}} > 30\,\mathrm{GeV}$, and $M_{\mathrm{T2}} > 125\,\mathrm{GeV}$ - called the high H_{T} region.

The M_{T2} requirement is chosen such that the expected contribution of the multijet background to the total SM background is negligible. For the low H_{T} region it is set to 200 GeV, as below that the M_{T2} distribution is distorted by the $E_{\mathrm{T}}^{\mathrm{miss}}$ requirement due to the trigger.

For each selected event, a pair of b jets is selected as we are searching for h^0 decay into $b\bar{b}$. To this purpose, the hemisphere division algorithm previously introduced (see Section 2) is used. The two b jets coming from the h^0 decay are expected to belong to the same hemisphere, since they both belong to the same decay branch and are expected to have a sizeable boost. The pair with the minimal angular distance $\Delta R(b_1, b_2) = \sqrt{(\Delta\phi)^2 + (\Delta\eta)^2}$ is selected if it satisfies $\Delta R(b_1, b_2) < 1.5$. In case no such pair is found within one hemisphere, we lift that constraint if the $\Delta R(b_1, b_2)$ requirement is still respected. This choice is made because the hemisphere division algorithm is not fully efficient, with an intrinsic inefficiency, which has been evaluated

---

[1] This is the only difference for b jets with respect to the inclusive M_{T2} analysis, where only b jets with $p_{\mathrm{T}} \geq 40\,\mathrm{GeV}$ are used.

as < 25% [13]. This inefficiency is due to the event configuration, like events where the Higgs boson is produced almost at rest, in which the two b jets can belong to different hemispheres.

The search is performed around the Higgs boson mass peak of $M_\mathrm{h} \sim 125\,\mathrm{GeV}$, but also the sideband region is used. Our search window thus reaches from $20 \leq M_\mathrm{bb} < 200\,\mathrm{GeV}$.

The overall yields of the main SM backgrounds (namely $t\bar{t}$+jets, $W(l\nu)$+jets, and $Z(\nu\bar{\nu})$+jets production) are estimated using the same methods as for the inclusive M_T2 analysis:

The $Z(\nu\bar{\nu})$+jets background is taken from simulation with an uncertainty of 100%. The simulation is validated in dileptonic events with $N_b \geq 2$ in the data.

For the lost-lepton background from $W(l\nu)$+jets and $t\bar{t}$+jets events, we apply the same background estimation method as for the inclusive M_T2 analysis using a one lepton data control sample. The shapes of M_bb distributions for the various backgrounds are obtained by simulation. We observe no appreciable dependence between M_T2 and M_bb, allowing us to obtain the shapes of M_bb from the high statistics distribution with relaxed M_T2. An uncertainty due to the relaxed M_T2 selection is taken into account. Further uncertainties on the shapes are assessed by varying several modelling parameters of the simulation, as it has been done for the inclusive M_T2 analysis.

Results are shown in Section 8.2.

8 Results

In Section 8.1 we first present the results of the inclusive M_T2 analysis based on the background estimates of Section 6. Then we also present the results of the M_T2 Higgs analysis in Section 8.2.

8.1 Results for the inclusive M_T2 analysis

Figures 7-9 show the M_T2 distributions in data corresponding to 19.5 fb^{-1} together with results of the various data-driven background estimates, separetely for all H_T and topological regions. The uncertainty on the background estimates is the quadratic sum of the statistical and systematic uncertainties. For the lost-lepton estimate we use simulation to obtain the shape. The tables and figures in this section do not display the shape uncertainty of the lost-lepton estimate. Table 2 shows the data in each signal region compared to the sum of the various data-driven background estimates.

Satisfactory agreement within the accuracy of the predictions is observed between the data and the data-driven estimates of the backgrounds. We evaluate the compatibility of the data and the standard model prediction by computing the pull value for every signal bin. The pull value is defined via

$$Pull = \frac{N_\mathrm{obs} - N_\mathrm{bkg}}{\sqrt{\sigma_\mathrm{obs}^2 + \sigma_\mathrm{bkg}^2}}, \tag{5}$$

where N_obs is the observed number of events with σ_obs its statistical uncertainty and N_bkg is the background estimate with a total uncertainty σ_bkg. A study using simulated pseudo-data shows that the observed pull distribution in data is compatible with the prediction with a probability of 11%.

A summary of the results of Figs. 7-9, summing up all M_T2 signal bins but keeping all topological and H_T signal region, is shown in Fig. 10.

Table 2: Estimated background event and data yields in all regions of the inclusive M_{T2} analysis. The uncertainties are the quadratic sum of statistical and systematic uncertainties.

signal region	low H_{T} region			medium H_{T} region			high H_{T} region		
	M_{T2} [GeV]	prediction	data	M_{T2} [GeV]	prediction	data	M_{T2} [GeV]	prediction	data
2 jets, 0 b jets	200 – 240	553±70	588	125 – 150	167±21	171	120 – 150	21.9±4.9	18
	240 – 290	395±53	451	150 – 180	128±17	104	150 – 200	19.4±4.3	18
	290 – 350	288±40	318	180 – 220	85.8±11.3	91	200 – 260	14.5±3.4	10
	350 – 420	236±52	232	220 – 270	70.0±10.3	78	260 – 350	6.3±1.8	9
	420 – 490	165±36	162	270 – 325	38.1±5.8	48	350 – 550	4.3±1.6	8
	490 – 570	68.9±15.5	61	325 – 425	43.4±10.1	45	≥ 550	3.0±1.4	6
	570 – 650	17.3±4.3	19	425 – 580	21.3±4.7	29			
	≥ 650	4.1±1.6	1	580 – 780	20.8±5.6	10			
				≥ 780	3.5±1.4	2			
2 jets, ≥1 b jets	200 – 250	56.4±12.8	56	100 – 135	27.4±9.6	30	100 – 180	11.4±8.1	2
	250 – 310	34.2±8.1	44	135 – 170	21.1±7.5	19	≥ 180	4.4±2.6	2
	310 – 380	25.9±7.4	29	170 – 260	13.4±5.4	15			
	380 – 450	19.9±5.8	13	260 – 450	7.3±3.5	7			
	450 – 550	12.6±3.8	15	≥ 450	3.4±1.7	9			
	≥ 550	2.6±0.8	3						
3-5 jets, 0 b jets	200 – 240	979±108	1041	160 – 185	243±23	234	160 – 185	34.9±4.7	39
	240 – 290	711±86	827	185 – 215	180±19	203	185 – 220	31.1±4.7	32
	290 – 350	492±65	522	215 – 250	134±16	152	220 – 270	25.5±4.3	25
	350 – 420	280±57	333	250 – 300	112±14	119	270 – 350	19.3±3.5	19
	420 – 490	138±29	145	300 – 370	89.0±12.2	91	350 – 450	9.1±2.5	6
	490 – 570	60.0±13.6	66	370 – 480	67.0±14.2	75	450 – 650	5.0±1.6	5
	570 – 650	13.8±3.9	21	480 – 640	35.0±8.0	40	≥ 650	4.4±1.6	5
	≥ 650	3.6±1.5	2	640 – 800	10.0±2.7	16			
				≥ 800	3.4±1.5	4			
3-5 jets, 1 b jets	200 – 250	305±34	300	150 – 175	93.4±10.7	87	150 – 180	13.5±3.1	28
	250 – 310	167±21	172	175 – 210	69.5±8.7	71	180 – 230	8.7±2.2	7
	310 – 380	103±16	98	210 – 270	52.8±6.8	63	230 – 350	6.2±1.6	9
	380 – 460	43.6±8.7	47	270 – 380	38.6±5.1	47	≥ 350	3.5±1.0	3
	460 – 550	17.9±4.1	19	380 – 600	15.9±3.2	19			
	≥ 550	4.0±1.1	4	≥ 600	3.6±0.9	4			
3-5 jets, 2 b jets	200 – 250	91.1±22.0	97	130 – 160	42.4±7.5	53	130 – 200	6.8±2.3	9
	250 – 325	52.7±13.7	39	160 – 200	26.5±5.5	29	≥ 200	2.9±1.1	6
	325 – 425	18.6±5.8	16	200 – 270	15.4±3.7	19			
	≥ 425	4.5±1.9	11	270 – 370	5.5±1.7	11			
				≥ 370	2.9±1.1	5			
≥ 6 jets, 0 b jets	200 – 280	50.8±8.9	56	160 – 200	38.5±6.2	44	160 – 200	12.1±2.9	12
	280 – 380	14.7±3.1	16	200 – 250	19.3±3.6	34	200 – 300	10.1±3.2	7
	≥ 380	7.3±2.3	8	250 – 325	14.1±2.8	23	≥ 300	4.5±1.7	2
				325 – 425	5.8±1.9	9			
				≥ 425	2.3±0.8	4			
≥ 6 jets, 1 b jets	200 – 250	32.0±6.7	31	150 – 190	38.7±5.9	38	150 – 200	7.3±3.2	6
	250 – 325	14.7±3.1	23	190 – 250	21.1±3.5	21	200 – 300	5.1±2.4	5
	≥ 325	4.8±1.5	11	250 – 350	10.5±1.9	13	≥ 300	2.3±1.1	1
				≥ 350	3.0±0.8	4			
≥ 6 jets, 2 b jets	200 – 250	12.0±4.3	15	130 – 170	41.0±7.0	54	130 – 200	10.6±6.0	10
	250 – 300	4.6±1.6	13	170 – 220	19.4±3.8	28	≥ 200	4.7±2.9	2
	≥ 300	2.8±1.0	6	220 – 300	10.4±2.1	8			
				≥ 300	4.3±0.8	6			
≥ 3 jets, ≥ 3 b jets	200 – 280	16.1±6.2	16	125 – 175	31.9±11.4	17	≥ 125	4.5±2.1	3
	≥ 280	4.6±1.7	7	175 – 275	16.1±6.3	13			
				≥ 275	6.1±2.4	1			

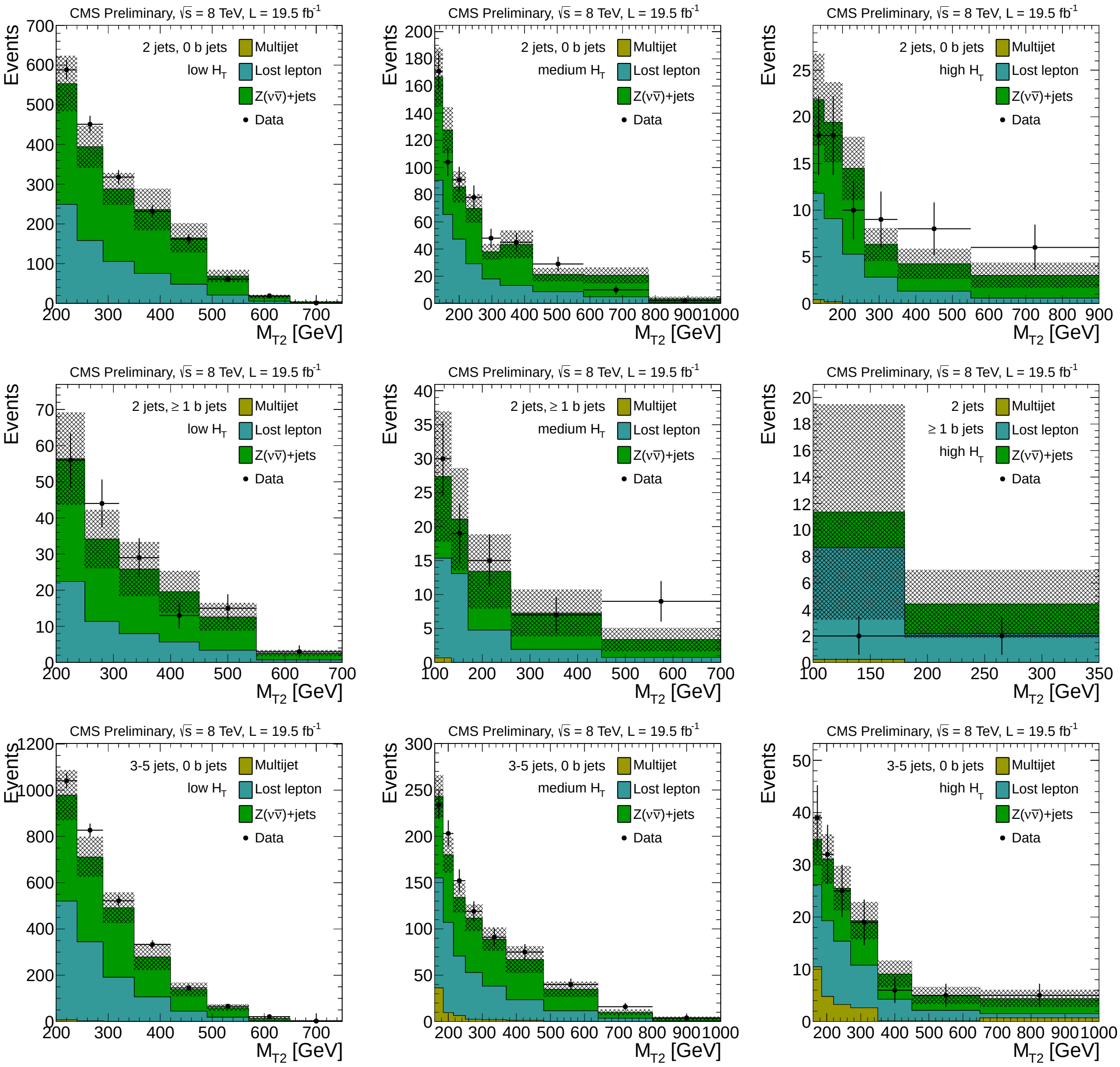

Figure 7: M_{T2} distributions from data-driven background estimates compared to data for low H_{T} (left), medium H_{T} (middle), and high H_{T} (right). The topological region in the jet − b-jet multiplicity is given in each plot. They are from top to bottom: $N_j = 2$ and $N_b = 0$, $N_j = 2$ and $N_b \geq 1$, $3 \leq N_j \leq 5$ and $N_b = 0$. The data correspond to an integrated luminosity of 19.5 fb^{-1}. All selection cuts are applied. The uncertainty band drawn in this figure does not contain shape uncertainties of the lost-lepton estimate.

8.2 Results for the M_{T2} Higgs analysis

Here we present the results for M_{T2} Higgs analysis, the search for $h^0 \rightarrow b\bar{b}$ produced within SUSY cascades.

The background is estimated as described in Section 7. Background predictions and the data yields are summarized in Table 3. Figure 11 shows the data-driven background prediction compared to data corresponding to 19.5 fb^{-1}. A possible signal distribution is also shown.

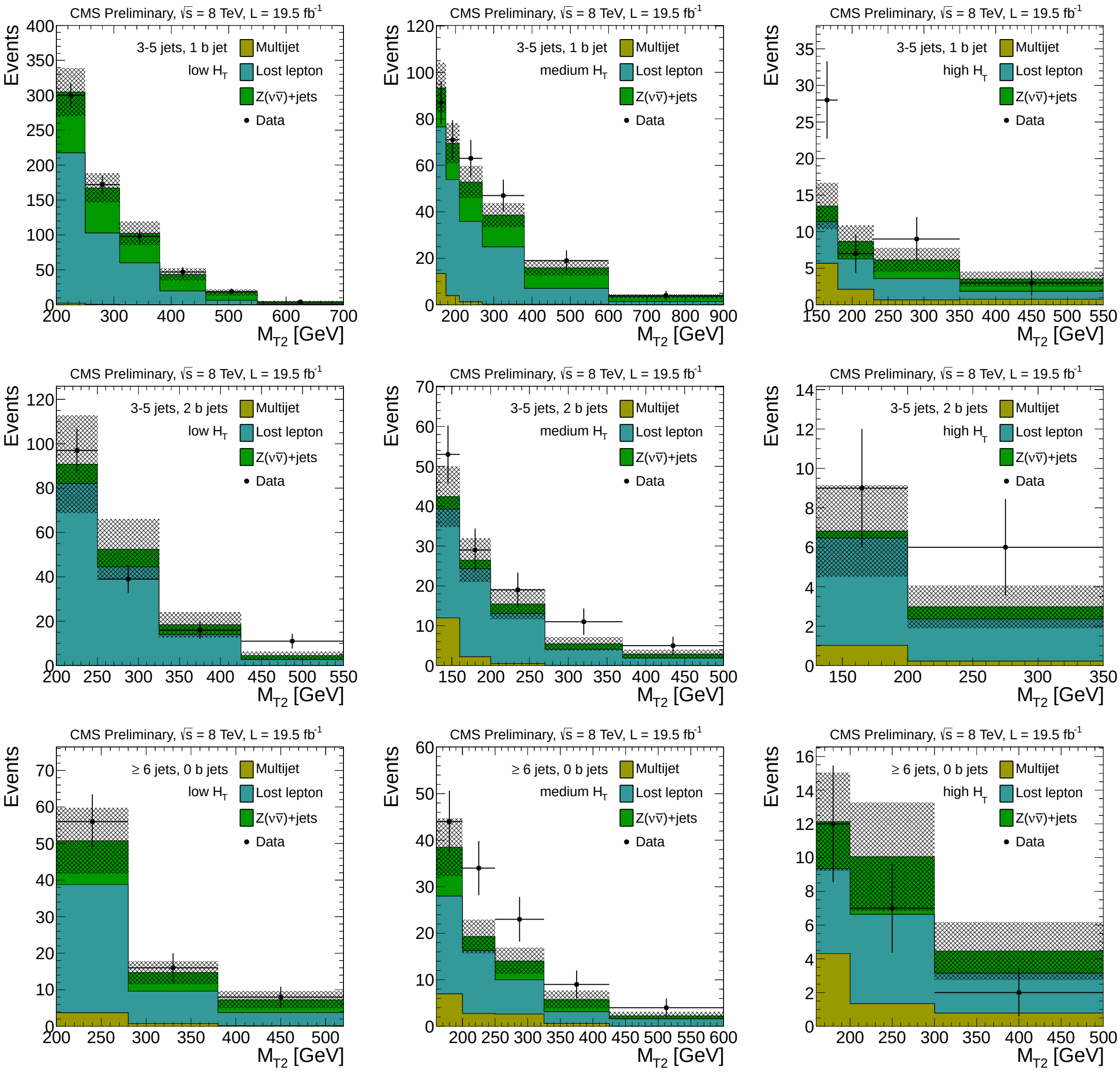

Figure 8: M_{T2} distributions from data-driven background estimates compared to data for low H_T (left), medium H_T (middle), and high H_T (right). The topological region in the jet − b-jet multiplicity is given in each plot. They are from top to bottom: $3 \leq N_j \leq 5$ and $N_b = 1$, $3 \leq N_j \leq 5$ and $N_b = 2$, $N_j \geq 6$ and $N_b = 0$. The data correspond to an integrated luminosity of 19.5 fb^{-1}. All selection cuts are applied. The uncertainty band drawn in this figure does not contain shape uncertainties of the lost-lepton estimate.

Table 3: Prediction of the $W(l\nu)$+jets and $t\bar{t}$+jets backgrounds from lost-lepton data estimate, and of the $Z(\nu\bar{\nu})$+jets background from simulation, for the low and high H_T regions within the mass range $20 \leq M_{bb} < 200\,\text{GeV}$, compared to data.

Channel	Lost lepton	$Z(\nu\bar{\nu})$+jets	Total background	Data
low H_T	37.1 ± 9.0	6.9 ± 6.9	44.0 ± 11.3	55
high H_T	64.8 ± 16.4	4.4 ± 4.4	69.2 ± 17.0	81

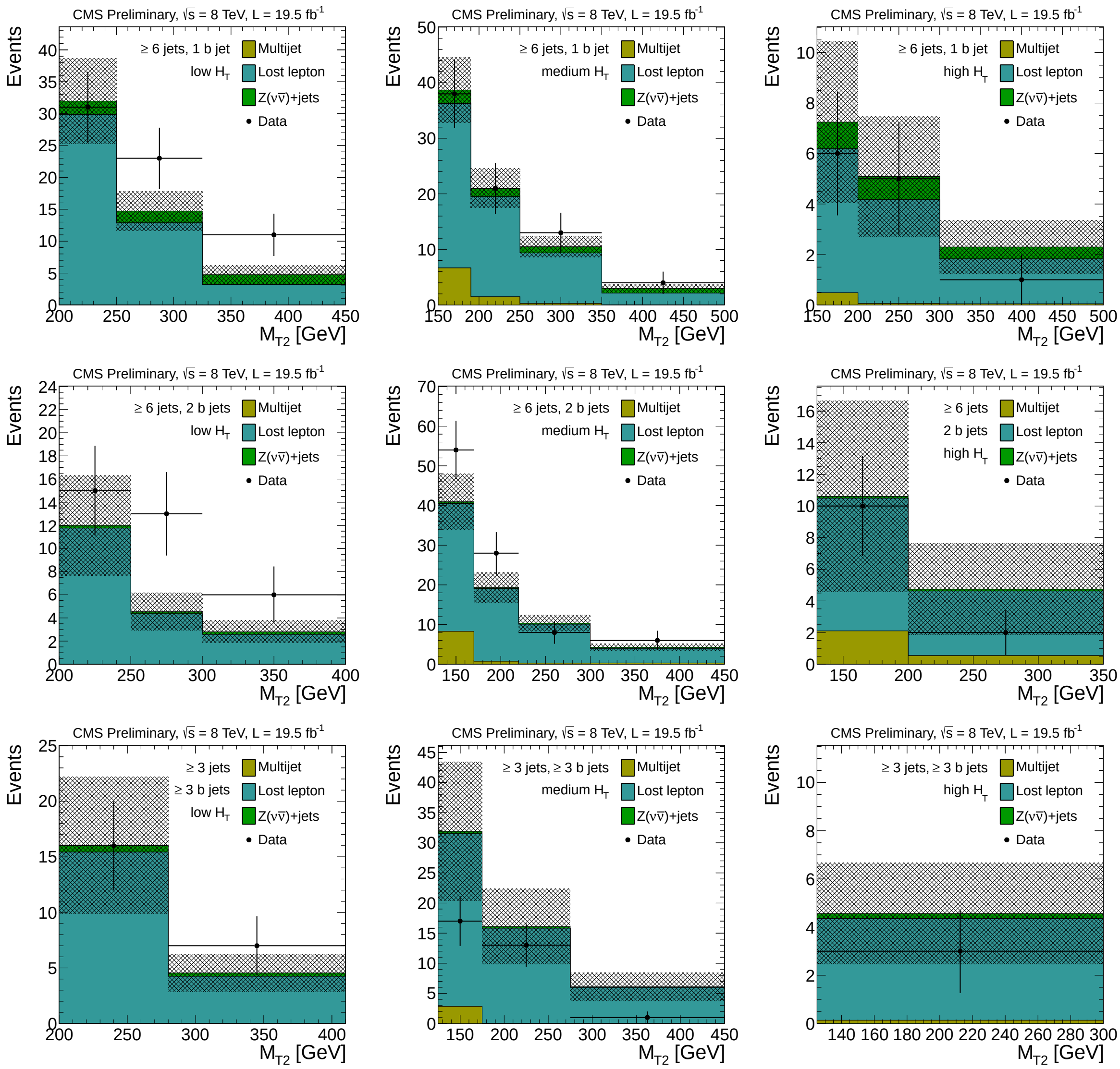

Figure 9: M_{T2} distribution from data-driven background estimates compared to data for low H_{T} (left), medium H_{T} (middle), and high H_{T} (right). The topological regions in the jet − b-jet multiplicity is given in each plot. They are from top to bottom: $N_j \geq 6$ and $N_b = 2$, $N_j \geq 6$ and $N_b = 2$, $N_j \geq 3$ and $N_b \geq 3$. The data correspond to an integrated luminosity of 19.5 fb^{-1}. All selection cuts are applied. The uncertainty band drawn in this figure does not contain shape uncertainties of the lost-lepton estimate.

9 Statistical interpretation of the results

Upper limits are set on a potential signal scenarios. A test on the background-only and signal+background hypotheses is performed using a modified frequentist approach, often referred to as CL_s [41, 42].

The contents of the low signal-to-background bins are important for the proper interpretation of the high signal-to-background bins. Therefore, a multi-bin approach is used in the analysis: We build a joint likelihood by comparing the observation with the background predictions in all signal bins. A likelihood function is constructed as the product of Poisson probabilities for each bin of N_j, N_b, H_{T}, and M_{T2}. The Poisson probabilities are functions of the number of observed events in each bin, n_i, and the predictions in each bin, λ_i, where i ranges from 1 to the

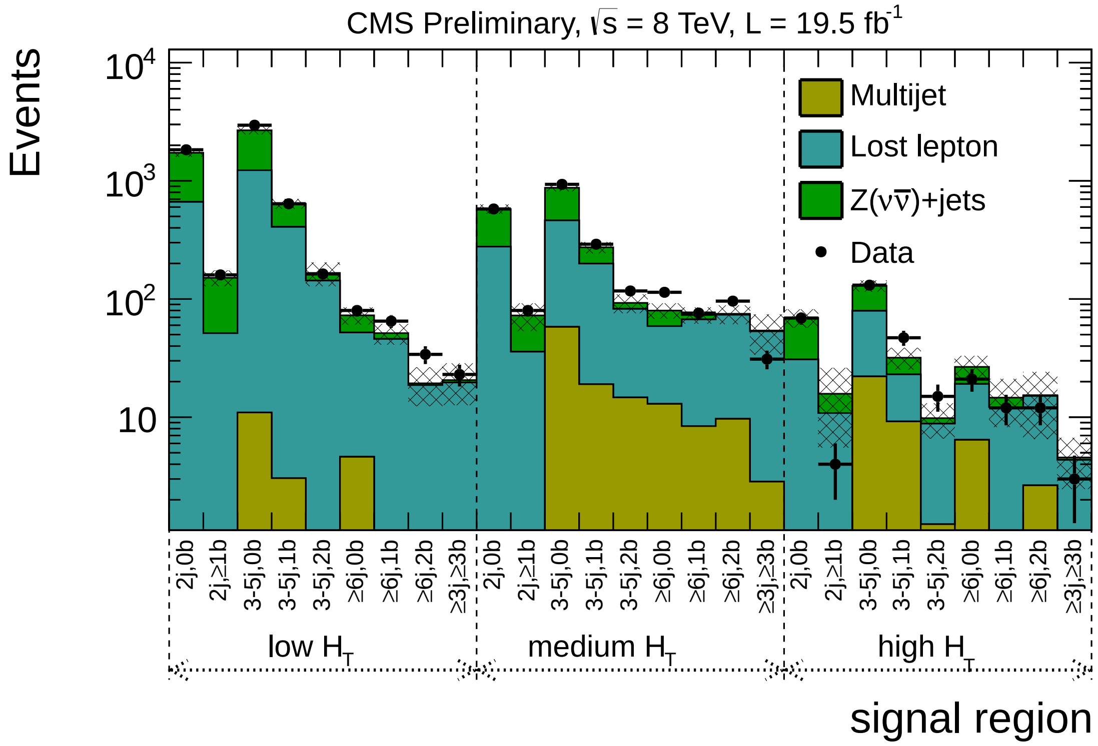

Figure 10: Results of the from data-driven background estimates compared to data for the three H_{T} signal regions as well as the topological regions in the jet $-$ b-jet multiplicity. The M_{T2} signal regions are summed up for each of the H_{T} and topological regions. The uncertainty band drawn in this figure does not contain shape uncertainties of the lost-lepton estimate. The data correspond to an integrated luminosity of 19.5 fb^{-1}. All selection cuts are applied.

number of bins, N_{bins}. The likelihood function is given by

$$\mathcal{L} = \prod_{i=1}^{N_{\mathrm{bins}}} \frac{\lambda_i^{n_i} e^{-\lambda_i}}{n_i!}. \tag{6}$$

The prediction in each bin is a sum over signal and background contributions:

$$\lambda_i = \mu \cdot s_i + \sum_{j=1}^{N_{\mathrm{bkg}}} b_{ij}, \tag{7}$$

where b_{ij} is the background prediction in bin i for background source j, s_i is the signal prediction in bin i, scaled by the signal strength modifier μ to test other values of the signal production cross section.

The uncertainties are handled by introducing nuisance parameters θ. The signal and background expectations, therefore, become dependent on N_{syst} nuisance parameters θ_m where $m = 1 \ldots N_{\mathrm{syst}}$: $s(\theta_m)$ and $b(\theta_m)$. All sources of uncertainties are taken to be either 100%-correlated (positively or negatively) or uncorrelated (independent), whichever is believed to be appropriate or more conservative. Incorporating the nuisance parameters, the likelihood function becomes:

$$\mathcal{L}(\mathrm{data}|\mu, \theta) = \mathrm{Poisson}(\mathrm{data}|\mu \cdot s(\theta) + b(\theta)) \cdot p(\theta), \tag{8}$$

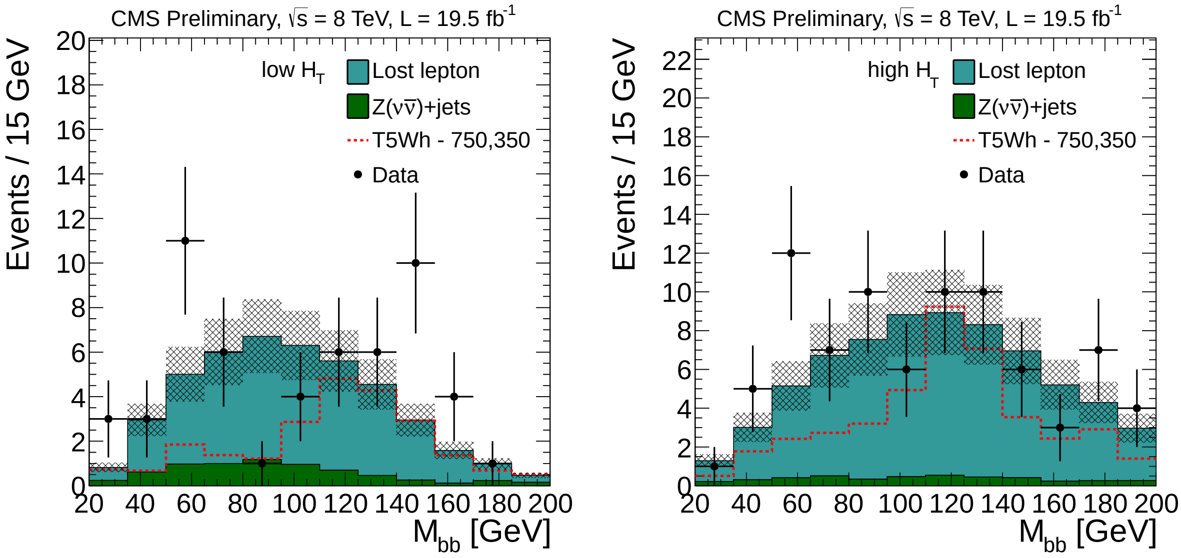

Figure 11: Standard model background estimation compared to data for low H_T (left) and high H_T (right), in the mass range $20 \leq M_\mathrm{bb} < 200\,\mathrm{GeV}$. The data correspond to an integrated luminosity of 19.5 fb^{-1}. All selection cuts are applied. A possible signal distribution (gluino-induced simplified model introduced in Section 10, $M_{\tilde{\mathrm{g}}} = 750\,\mathrm{GeV}, M_\mathrm{LSP} = 350\,\mathrm{GeV}$) is also shown, as a dashed line. The uncertainty band drawn in this figure does not contain shape uncertainties of the lost-lepton estimate.

where $p(\theta)$ is the probability density function (pdf) associated to the given systematic uncertainty. Lognormal pdfs are assumed, a more suitable alternative than the truncated Gaussian, in order to describe positively defined parameters. They are characterized by parameter $\kappa = 1 + \epsilon$, where ϵ represents the relative uncertainty for a Gaussian distribution.

In order to compare the compatibility of the data with the background-only and the signal+background hypotheses we construct the test statistic q_μ [43] based on the profile-likelihood ratio:

$$q_\mu = -2\ln\frac{\mathcal{L}(\mathrm{data}|\mu,\hat{\theta}_\mu)}{\mathcal{L}(\mathrm{data}|\hat{\mu},\hat{\theta})}, \qquad \text{with } 0 \leq \hat{\mu} \leq \mu \tag{9}$$

where “data” can be the actual data observation or pseudo-data. Both the denominator and the numerator are maximized. In the numerator, the signal parameter strength μ remains fixed and the likelihood is maximized for only the nuisance parameters, which values at the maximum is denoted as $\hat{\theta}_\mu$. In the denominator, the likelihood is maximized for both μ and θ and $\hat{\mu}$ and $\hat{\theta}$ are the values, at which $\mathcal{L}$ reaches its global maximum. The lower constraint $0 \leq \hat{\mu}$ is imposed as the signal strength cannot be negative, while the upper constraint guarantees a one-sided confidence interval (physics-wise, this means that upward fluctuations of data are not considered as evidence against the signal hypothesis). The value of the test statistic for the actual observation is denoted as q_μ^obs. This test statistic, defined by the LHC Higgs Combination group [44], differs from what has been used at LEP and Tevatron.

For the limit setting, a modified frequentist $\mathrm{CL_s}$ approach is used. Probabilities, or p-values, of observing an outcome of an experiment at least as signal-like as the one observed are calculated for the null (background-only) hypothesis H_0 and for the test (signal+background) hypothesis

H_1:

$$\begin{aligned} \mathrm{CL}_{s+b} &= P(q_\mu \geq q_\mu^{\mathrm{obs}} | H_1), \\ \mathrm{CL}_b &= P(q_\mu \geq q_\mu^{\mathrm{obs}} | H_0). \end{aligned} \tag{10}$$

The CL_s quantity is then defined as the ratio of these probabilities:

$$\mathrm{CL}_s = \frac{\mathrm{CL}_{s+b}}{\mathrm{CL}_b}. \tag{11}$$

In the modified frequentist approach, the value CL_s is required to be less than or equal to α in order to declare a $(1-\alpha)$ C.L. exclusion.

In practice, the p-values of the background-only and the signal+background hypotheses are determined from distributions of the test-statistic constructed from simulated pseudo-experiments. Once the ensembles of pseudo-experiments for the two hypotheses are generated, the observed CL_s limit is calculated from these distributions and the actual observation of the test-statistic q_μ^{obs}. The expected CL_s limit is calculated by replacing q_μ^{obs} by the expected median from the distribution of the background-only hypothesis. The limits are computed following the LHC Higgs Combination prescription [44] .

10 Exclusion limits

A 95% C.L. upper limit on the number of events has been computed using the CL_s formulation described in Section 9. The systematic uncertainties on the background predictions have been discussed in the corresponding sections. The dominant sources of systematic uncertainties on the signal model are found to be the jet energy scale [32], the b-tagging efficiency [35] and the p_T MC NLO uncertainty [37]. A systematic uncertainty associated with the parton distribution functions have been also evaluated following the prescription of the PDF4LHC group [45]. Additionally, uncertainties associated with the luminosity determination [46] and the trigger efficiency have been considered. A summary of the range of effect of each source of systematic uncertainty can be found in Table 4.

The effect of signal contamination in the leptonic control region could be significant and has been taken into account in the limit setting by propagating the signal contribution in the lost-lepton control region to the hadronic signal region and subtracting its effect.

The method determines the fraction, μ, of the signal within the acceptance that is excluded. A resulting fraction $\mu \leq 1$ implies that the tested signal is excluded.

10.1 Exclusion limits in simplified models

In this section we interpret the results of our search in terms of simplified models [7] that allow to compare the exclusion potential in the context of a larger variety of fundamental models, not necessarily in the MSSM framework. We studied the following topologies:

For the inclusive M_{T2} analysis:

- Direct squark production with $\tilde{q} \to q\tilde{\chi}_1^0$. The topological regions used are $N_j = 2$ and $N_b = 0$, $N_j = 2$ and $N_b \geq 1$, $3 \leq N_j \leq 5$ and $N_b = 0$, $3 \leq N_j \leq 5$ and $N_b = 1$, $N_j \geq 6$ and $N_b = 0$. Exclusions limits are shown in Fig. 12a, with a scenario where the first two generations of squarks ($\tilde{u}_\mathrm{L}$, $\tilde{u}_\mathrm{R}$, $\tilde{d}_\mathrm{L}$, $\tilde{d}_\mathrm{R}$, $\tilde{c}_\mathrm{L}$, $\tilde{c}_\mathrm{R}$, $\tilde{s}_\mathrm{L}$, $\tilde{s}_\mathrm{R}$) are degenerate and light, and another scenario corresponding to only one light flavor accessible squark.

Table 4: Summary of systematic uncertainties with typical ranges of effect.

Process	Source/Region	Effect	Shape
Multijet	$M_{\mathrm{T2}} < 200\,\mathrm{GeV}$	10-50%	–
	$M_{\mathrm{T2}} \geq 200\,\mathrm{GeV}$	50-100%	–
$W(l\nu)$+jets and Top	Lost-lepton method	10-65%	–
	b-tagging scale factor	–	x
	Jet energy scale	–	x
	Matching scale	–	x
	Renormalization and factorization scale	–	x
	p_{T} MC NLO uncertainty	–	x
$Z(\nu\bar{\nu})$+jets	Systematics on $Z(\nu\bar{\nu})/\gamma$ ratio (0-1 b jets)	20-30%	–
	Systematics on $1b/0b$ ratio from Z_{ll} (1 b jet)	10-75%	–
	Statistics from γ+jets data (0-1 b jet)	5-100%	–
	simulation ($\geq$ 2 b jets)	100%	–
Signal	Luminosity uncertainty	2.6%	–
	Trigger efficiency	1%	–
	Parton distribution functions	5-15%	–
	b-tagging scale factor	5-40%	x
	Jet energy scale	5-40%	x
	p_{T} MC NLO uncertainty	10-20%	x

- Direct pair production of sbottom with $\tilde{b} \to b\tilde{\chi}^0_1$. The topological regions used are $N_j = 2$ and $N_b \geq 1$, $3 \leq N_j \leq 5$ and $N_b = 1$, $3 \leq N_j \leq 5$ and $N_b = 2$. Exclusions limits are shown in Fig. 12b.
- Direct pair production of stop with $\tilde{t} \to t\tilde{\chi}^0_1$. The topological regions used are $3 \leq N_j \leq 5$ and $N_b = 1$, $3 \leq N_j \leq 5$ and $N_b = 2$, $N_j \geq 6$ and $N_b = 1$, $N_j \geq 6$ and $N_b = 2$, $N_j \geq 3$ and $N_b \geq 3$. Exclusions limits are shown in Fig. 12c.
- Gluino pair production, with $\tilde{g} \to q\bar{q}\tilde{\chi}^0_1$. The topological regions used are $3 \leq N_j \leq 5$ and $N_b = 0$, $3 \leq N_j \leq 5$ and $N_b = 1$, $N_j \geq 6$ and $N_b = 0$, $N_j \geq 6$ and $N_b = 1$. Exclusions limits are shown in Fig. 13a.
- Gluino pair production, with $\tilde{g} \to b\bar{b}\tilde{\chi}^0_1$. The topological regions used are $3 \leq N_j \leq 5$ and $N_b = 1$, $3 \leq N_j \leq 5$ and $N_b = 2$, $N_j \geq 6$ and $N_b = 1$, $N_j \geq 6$ and $N_b = 2$, $N_j \geq 3$ and $N_b \geq 3$. Exclusions limits are shown in Fig. 13b.
- Gluino pair production, with $\tilde{g} \to t\bar{t}\tilde{\chi}^0_1$. The topological regions used are $N_j \geq 6$ and $N_b = 1$, $N_j \geq 6$ and $N_b = 2$, $N_j \geq 3$ and $N_b \geq 3$. Exclusions limits are shown in Fig. 13c.

For the M_{T2} Higgs analysis:

- Gluino pair production with one gluino decaying via $\tilde{g} \to q\bar{q}\tilde{\chi}^0_2$, $\tilde{\chi}^0_2 \to h^0\tilde{\chi}^0_1$, while the other gluino decaying via $\tilde{g} \to qq'\tilde{\chi}^\pm_1$, $\tilde{\chi}^\pm_1 \to W^\pm\tilde{\chi}^0_1$. In this scenario, neutralino $\tilde{\chi}^0_2$ and chargino $\tilde{\chi}^\pm_1$ are degenerate, with a mass:

  $$M(\tilde{\chi}^0_2) = M(\tilde{\chi}^\pm_1) = M(\tilde{\chi}^0_1) + 200\,\mathrm{GeV}.$$

  Exclusions limits are shown in Fig. 14.

The observed limit differs from expected limit for the simplified model of direct pair production of stop with $\tilde{t} \to t\tilde{\chi}^0_1$. Simulation suggests that this is not due to an overfluctuation in the signal region, but rather an underfluctuation in the leptonic control region leading to a too small data prediction. Taking into account the number of data control regions (there are 81 leptonic control regions) the probability of such a fluctuation has been evaluated to be $\sim$ 65%.

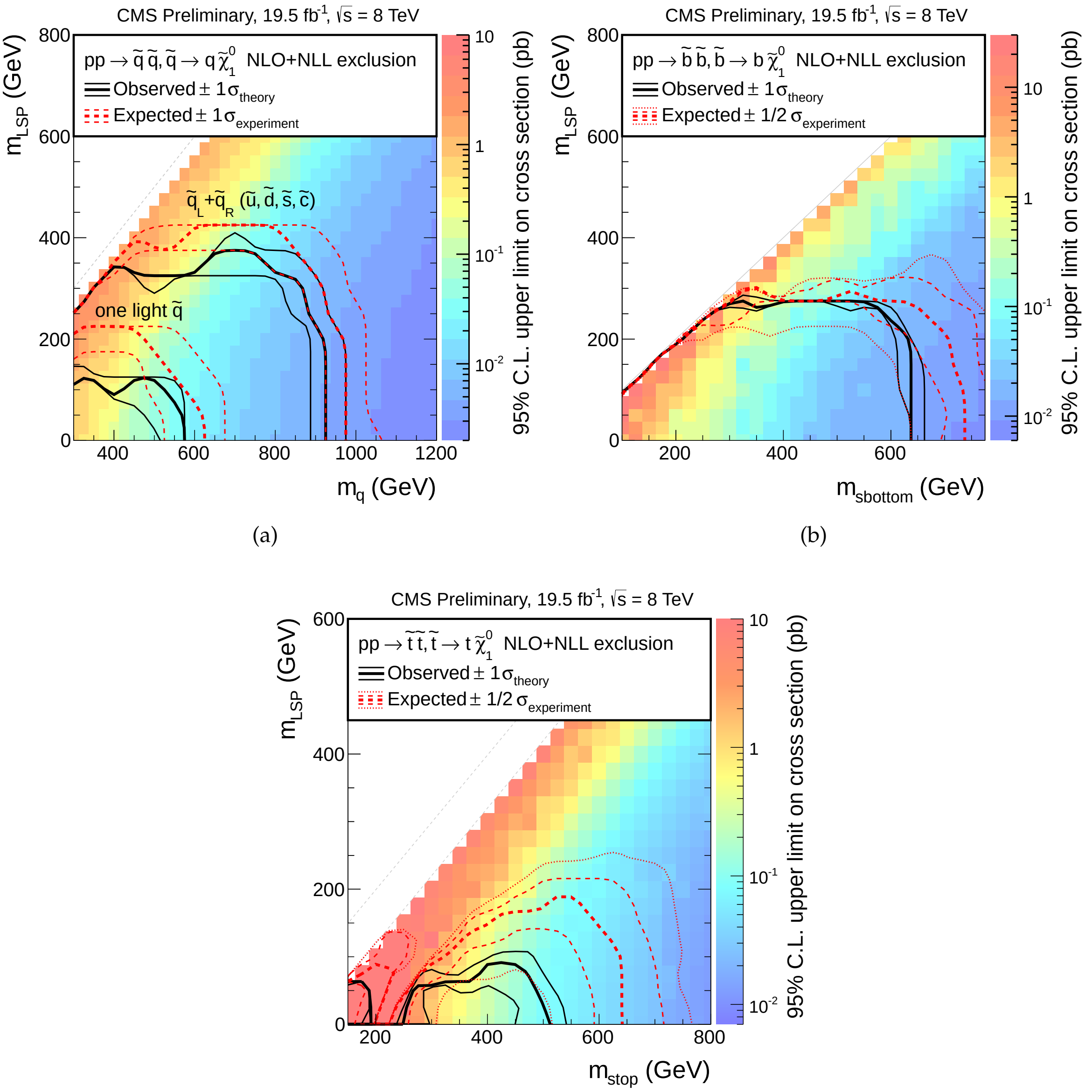

(a) (b)

(c)

Figure 12: Exclusion limits for (a) direct squark production, (b) direct sbottom production, and (c) direct stop production. For the direct squark production, the upper set of curves corresponds to the scenario where the first two generations of squarks are degenerate and light, while the lower set corresponds to only one accessible light flavor squark.

In Table 5 we summarize the exclusion limits we observe from Figs. 12, 13, and 14. The limits quoted here are the observed limit minus one standard deviation σ_{theory}.

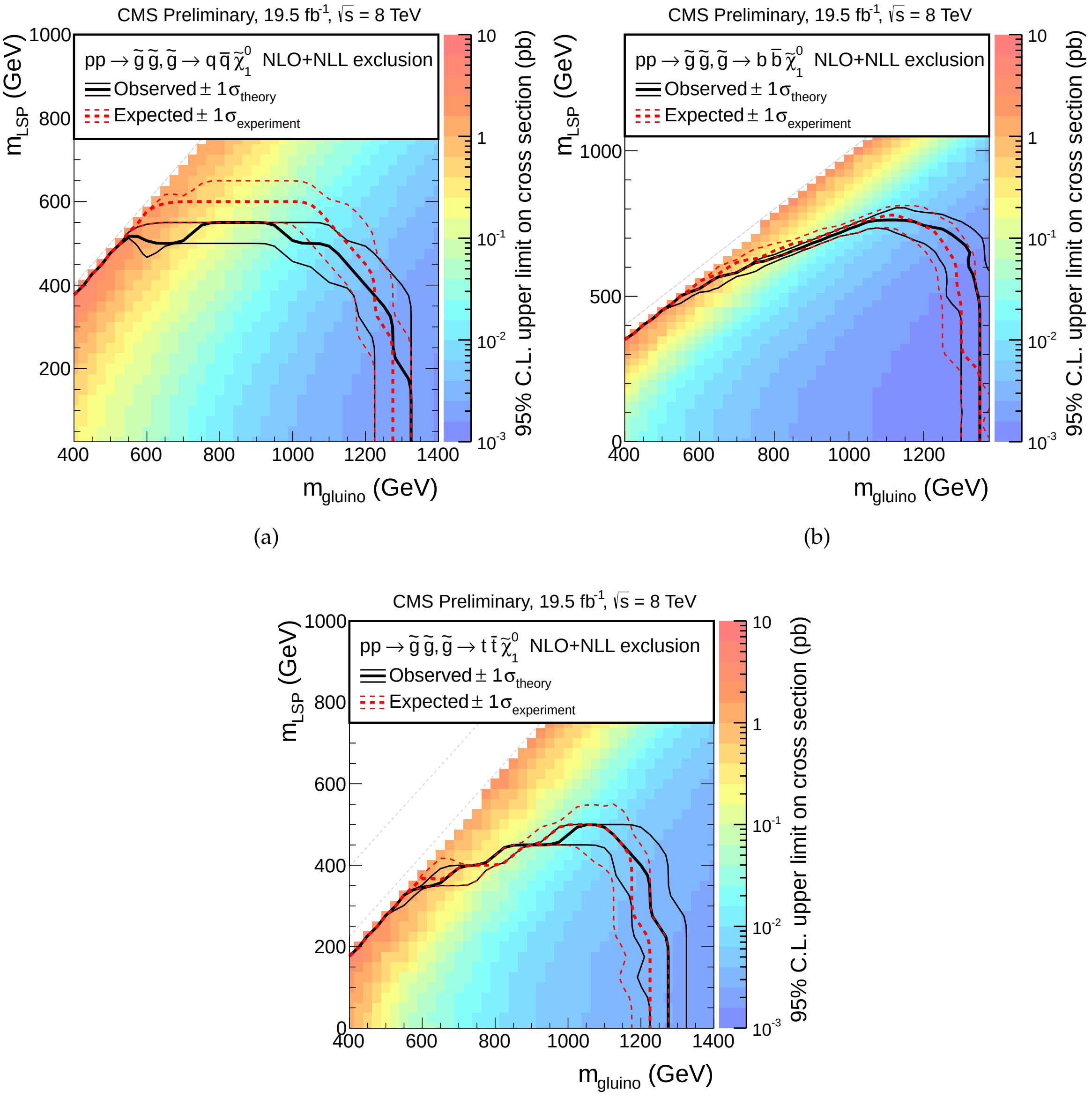

(a)

(b)

(c)

Figure 13: Exclusion limits for gluino mediated (a) squark production, (b) sbottom production, and (c) stop production. The squarks are highly virtual, thus the gluinos giving rise to three body decays.

11 Conclusion

As a continuation of and improvement over the published analysis at 7 TeV, the data taken with the CMS detector during the 2012 LHC run have been analyzed using the M_{T2} approach. Hadronic H_T triggers and E_T^{miss} triggers are used to select the candidate events. A cleaning procedure is applied in order to remove events containing instrumental noise and/or potentially fake E_T^{miss}.

The main approach, the inclusive M_{T2} analysis, targets a broad spectrum of SUSY models with R-parity conservation, that comes naturally with sizeable E_T^{miss}. Events containing a lepton are vetoed to suppress electroweak ($W(l\nu)$+jets and $Z(ll)$+jets) processes and top ($t\bar{t}$+jets and

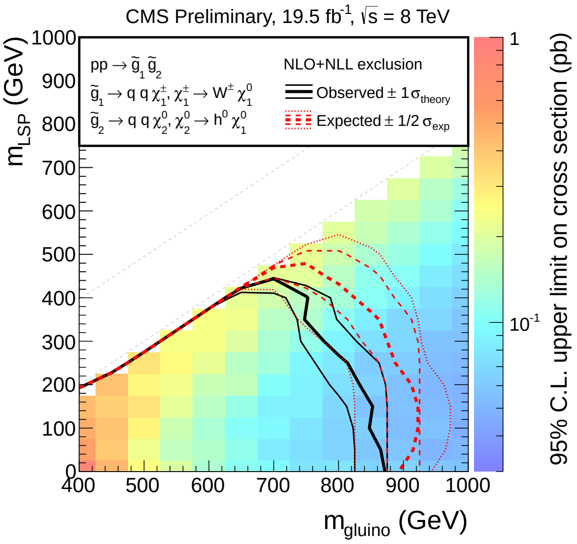

Figure 14: Exclusion limits for gluino pair production with one gluino decaying via $\tilde{g} \to q\bar{q}\tilde{\chi}_2^0$, $\tilde{\chi}_2^0 \to h^0\tilde{\chi}_1^0$, while the other gluino decaying via $\tilde{g} \to qq'\tilde{\chi}_1^{\pm}$, $\tilde{\chi}_1^{\pm} \to W^{\pm}\tilde{\chi}_1^0$.

Table 5: Summary of observed mass limits (at 95% C.L.) in different simplified models. The limits quoted here are the observed limit minus one standard deviation σ_{theory}. The limit on the parent mass is quoted at $M_{\text{LSP}} = 0$, the limit on the LSP mass is taken as the best limit. The limit on the mass splitting of parent and LSP is taken, where the splitting is the smallest.

simplified model	limit on parent mass at $M_{\text{LSP}} = 0$	best limit on LSP mass	lower limit on mass splitting parent − LSP
direct squark production			
single light squark	$M_{\tilde{q}} < 520\,\text{GeV}$	$M_{\text{LSP}} < 120\,\text{GeV}$	$\Delta M(\tilde{q},\tilde{\chi}_1^0) > 200\,\text{GeV}$
8 degenerate light squarks	$M_{\tilde{q}} < 875\,\text{GeV}$	$M_{\text{LSP}} < 325\,\text{GeV}$	$\Delta M(\tilde{q},\tilde{\chi}_1^0) > 50\,\text{GeV}$
direct sbottom production	$M_{\tilde{b}} < 640\,\text{GeV}$	$M_{\text{LSP}} < 275\,\text{GeV}$	$\Delta M(\tilde{b},\tilde{\chi}_1^0) > 10\,\text{GeV}$
direct stop production			
$M_{\text{stop}} > M_{\text{top}} + M_{\text{LSP}}$	$300 < M_{\tilde{t}} < 450\,\text{GeV}$	$M_{\text{LSP}} < 60\,\text{GeV}$	$\Delta M(\tilde{t},\tilde{\chi}_1^0) > 230\,\text{GeV}$
$M_{\text{stop}} < M_{\text{top}} + M_{\text{LSP}}$	$M_{\tilde{t}} < 175\,\text{GeV}$	$M_{\text{LSP}} < 60\,\text{GeV}$	$\Delta M(\tilde{t},\tilde{\chi}_1^0) > 90\,\text{GeV}$
direct gluino production			
$\tilde{g} \to q\bar{q}\tilde{\chi}_1^0$	$M_{\tilde{g}} < 1225\,\text{GeV}$	$M_{\text{LSP}} < 510\,\text{GeV}$	$\Delta M(\tilde{g},\tilde{\chi}_1^0) > 25\,\text{GeV}$
$\tilde{g} \to b\bar{b}\tilde{\chi}_1^0$	$M_{\tilde{g}} < 1300\,\text{GeV}$	$M_{\text{LSP}} < 740\,\text{GeV}$	$\Delta M(\tilde{g},\tilde{\chi}_1^0) > 50\,\text{GeV}$
$\tilde{g} \to t\bar{t}\tilde{\chi}_1^0$	$M_{\tilde{g}} < 1225\,\text{GeV}$	$M_{\text{LSP}} < 450\,\text{GeV}$	$\Delta M(\tilde{g},\tilde{\chi}_1^0) > 225\,\text{GeV}$
direct gluino production $\tilde{g}_1 \to q\bar{q}\tilde{\chi}_2^0$, $\tilde{\chi}_2^0 \to h^0\tilde{\chi}_1^0$, $\tilde{g}_2 \to qq'\tilde{\chi}_1^{\pm}$, $\chi_1^{\pm} \to W^{\pm}\tilde{\chi}_1^0$	$M_{\tilde{g}} < 825\,\text{GeV}$	$M_{\text{LSP}} < 410\,\text{GeV}$	$\Delta M(\tilde{g},\tilde{\chi}_1^0) > 225\,\text{GeV}$

single top) production. The analysis is based on multijet events with at least two jets. In order to gain sensitivity for various production and decay modes we select nine exclusive signal regions depending on the jet and b-jet multiplicity. Three disjoint H_{T} regions are defined that target a broad spectrum of masses and mass splittings. Finally, the data are analyzed in up to nine bins in M_{T2}, the number of bins depending on the event statistics in the various regions. The SM background prediction is performed by means of data-driven estimations. The tail of the M_{T2} distribution, obtained after this selection, is sensitive to a potential SUSY signal. No significant excess beyond the SM expectations has been found in 19.5 fb^{-1} of data.

A second line of approach, the M_{T2} Higgs analysis, targets SUSY models with a light Higgs boson produced within SUSY cascades. Typically, squarks and gluinos may decay to $\tilde{\chi}_2^0$, which in turn has a large branching fraction to $h^0\tilde{\chi}_1^0$ in large regions of the MSSM parameter space. The dominant Higgs boson decay mode $h^0 \rightarrow b\bar{b}$ is analyzed. A method is presented to select two b jets in order to reach high signal selection efficiency of $b\bar{b}$ pairs coming from the Higgs boson decay. The signal is extracted out of the invariant mass the selected b pairs. The SM background prediction is performed by means of data-driven estimations.

No excess beyond the SM expectations has been found in 19.5 fb^{-1} of data. Exlusion limits on simplied model scans are set.

References

[1] S. P. Martin, "A Supersymmetry primer", `arXiv:hep-ph/9709356`.

[2] C. Lester and D. Summers, "Measuring masses of semiinvisibly decaying particles pair produced at hadron colliders", *Phys.Lett.* **B463** (1999) 99–103, `doi:10.1016/S0370-2693(99)00945-4`, `arXiv:hep-ph/9906349`.

[3] CDF Collaboration, "Top Quark Mass Measurement using mT2 in the Dilepton Channel at CDF", *Phys.Rev.* **D81** (2010) 031102, `doi:10.1103/PhysRevD.81.031102`, `arXiv:0911.2956`.

[4] ATLAS Collaboration, "Search for a heavy top-quark partner in final states with two leptons with the ATLAS detector at the LHC", *JHEP* **1211** (2012) 094, `doi:10.1007/JHEP11(2012)094`, `arXiv:1209.4186`.

[5] ATLAS Collaboration, "Search for direct slepton and gaugino production in final states with two leptons and missing transverse momentum with the ATLAS detector in pp collisions at $\sqrt{s} = 7$ TeV", *Phys.Lett.* **B718** (2013) 879–901, `doi:10.1016/j.physletb.2012.11.058`, `arXiv:1208.2884`.

[6] CMS Collaboration, "Search for supersymmetry in hadronic final states using M_{T2} in pp collisions at $\sqrt{s} = 7$ TeV", *JHEP* **1210** (2012) 018, `doi:10.1007/JHEP10(2012)018`, `arXiv:1207.1798`.

[7] LHC New Physics Working Group Collaboration, "Simplified Models for LHC New Physics Searches", *J.Phys.* **G39** (2012) 105005, `doi:10.1088/0954-3899/39/10/105005`, `arXiv:1105.2838`.

[8] ATLAS Collaboration, "Search for direct third-generation squark pair production in final states with missing transverse momentum and two b-jets in $\sqrt{s} = 8$ TeV pp collisions with the ATLAS detector", *JHEP* **1310** (2013) 189, `doi:10.1007/JHEP10(2013)189`, `arXiv:1308.2631`.

[9] ATLAS Collaboration, "Search for new phenomena in final states with large jet multiplicities and missing transverse momentum at $\sqrt{s} = 8$ TeV proton-proton collisions using the ATLAS experiment", *JHEP* **1310** (2013) 130, `doi:10.1007/JHEP10(2013)130`, `arXiv:1308.1841`.

[10] CMS Collaboration, "Search for supersymmetry in hadronic final states with missing transverse energy using the variables AlphaT and b-quark multiplicity in pp collisions at 8 TeV", *Eur.Phys.J.* **C73** (2013) 2568, `doi:10.1140/epjc/s10052-013-2568-6`, `arXiv:1303.2985`.

[11] CMS Collaboration, "Search for gluino mediated bottom- and top-squark production in multijet final states in pp collisions at 8 TeV", *Phys.Lett.* **B725** (2013) 243–270, `doi:10.1016/j.physletb.2013.06.058`, `arXiv:1305.2390`.

[12] H.-C. Cheng and Z. Han, "Minimal Kinematic Constraints and m(T2)", *JHEP* **0812** (2008) 063, `doi:10.1088/1126-6708/2008/12/063`, `arXiv:0810.5178`.

[13] CMS Collaboration, "CMS technical design report, volume II: Physics performance", *J.Phys.* **G34** (2007) 995–1579, `doi:10.1088/0954-3899/34/6/S01`.

[14] T. Sjostrand, S. Mrenna, and P. Z. Skands, "PYTHIA 6.4 Physics and Manual", *JHEP* **0605** (2006) 026, `doi:10.1088/1126-6708/2006/05/026`, `arXiv:hep-ph/0603175`.

[15] CMS Collaboration, "The CMS experiment at the CERN LHC", *JINST* **3** (2008) S08004, `doi:10.1088/1748-0221/3/08/S08004`.

[16] J. Alwall et al., "MadGraph 5 : Going Beyond", *JHEP* **1106** (2011) 128, `doi:10.1007/JHEP06(2011)128`, `arXiv:1106.0522`.

[17] E. Re, "Single-top Wt-channel production matched with parton showers using the POWHEG method", *Eur.Phys.J.* **C71** (2011) 1547, `doi:10.1140/epjc/s10052-011-1547-z`, `arXiv:1009.2450`.

[18] P. M. Nadolsky et al., "Implications of CTEQ global analysis for collider observables", *Phys.Rev.* **D78** (2008) 013004, `doi:10.1103/PhysRevD.78.013004`, `arXiv:0802.0007`.

[19] GEANT4 Collaboration, "GEANT4: A Simulation toolkit", *Nucl.Instrum.Meth.* **A506** (2003) 250–303, `doi:10.1016/S0168-9002(03)01368-8`.

[20] W. Beenakker, R. Hopker, M. Spira, and P. Zerwas, "Squark and gluino production at hadron colliders", *Nucl.Phys.* **B492** (1997) 51–103, `doi:10.1016/S0550-3213(97)80027-2`, `arXiv:hep-ph/9610490`.

[21] A. Kulesza and L. Motyka, "Threshold resummation for squark-antisquark and gluino-pair production at the LHC", *Phys.Rev.Lett.* **102** (2009) 111802, `doi:10.1103/PhysRevLett.102.111802`, `arXiv:0807.2405`.

[22] A. Kulesza and L. Motyka, "Soft gluon resummation for the production of gluino-gluino and squark-antisquark pairs at the LHC", *Phys.Rev.* **D80** (2009) 095004, `doi:10.1103/PhysRevD.80.095004`, `arXiv:0905.4749`.

[23] W. Beenakker et al., "Soft-gluon resummation for squark and gluino hadroproduction", *JHEP* **0912** (2009) 041, `doi:10.1088/1126-6708/2009/12/041`, `arXiv:0909.4418`.

[24] W. Beenakker et al., "Squark and Gluino Hadroproduction", *Int.J.Mod.Phys.* **A26** (2011) 2637–2664, `doi:10.1142/S0217751X11053560`, `arXiv:1105.1110`.

[25] M. Kramer et al., "Supersymmetry production cross sections in pp collisions at $\sqrt{s} = 7$ TeV", `arXiv:1206.2892`.

[26] CMS Collaboration, "Particle-Flow Event Reconstruction in CMS and Performance for Jets, Taus, and MET", *CMS-PAS* **PFT-09-001** (2009).

[27] CMS Collaboration, "Electron reconstruction and identification at $\sqrt{s} = 7$ TeV", *CMS-PAS* **EGM-10-004** (2010).

[28] CMS Collaboration Collaboration, "Performance of CMS muon reconstruction in pp collision events at $\sqrt{s} = 7$ TeV", *JINST* **7** (2012) P10002, `doi:10.1088/1748-0221/7/10/P10002`, `arXiv:1206.4071`.

[29] M. Cacciari, G. P. Salam, and G. Soyez, "The Anti-k_t jet clustering algorithm", *JHEP* **0804** (2008) 063, `doi:10.1088/1126-6708/2008/04/063`, `arXiv:0802.1189`.

[30] CMS Collaboration, "Jet Performance in pp Collisions at 7 TeV", *CMS-PAS* **JME-10-003** (2010).

[31] CMS Collaboration, "Commissioning of the Particle-Flow reconstruction in Minimum-Bias and Jet Events from pp Collisions at 7 TeV", *CMS-PAS* **PFT-10-002** (2010).

[32] CMS Collaboration, "Determination of Jet Energy Calibration and Transverse Momentum Resolution in CMS", *JINST* **6** (2011) P11002, `doi:10.1088/1748-0221/6/11/P11002`, `arXiv:1107.4277`.

[33] M. Cacciari and G. P. Salam, "Pileup subtraction using jet areas", *Phys.Lett.* **B659** (2008) 119–126, `doi:10.1016/j.physletb.2007.09.077`, `arXiv:0707.1378`.

[34] M. Cacciari, G. P. Salam, and G. Soyez, "The Catchment Area of Jets", *JHEP* **0804** (2008) 005, `doi:10.1088/1126-6708/2008/04/005`, `arXiv:0802.1188`.

[35] CMS Collaboration, "Identification of b-quark jets with the CMS experiment", *JINST* **8** (2013) P04013, `doi:10.1088/1748-0221/8/04/P04013`, `arXiv:1211.4462`.

[36] CMS Collaboration, "Tracking and Primary Vertex Results in First 7 TeV Collisions", *CMS-PAS* **TRK-10-005** (2010).

[37] CMS Collaboration, "Search for top-squark pair production in the single-lepton final state in pp collisions at sqrt(s) = 8 TeV", `arXiv:1308.1586`.

[38] S. Ask et al., "Using gamma+jets Production to Calibrate the Standard Model Z(nunu)+jets Background to New Physics Processes at the LHC", *JHEP* **1110** (2011) 058, `doi:10.1007/JHEP10(2011)058`, `arXiv:1107.2803`.

[39] S. Abdullin and D. Denegri, "On the Possibility to Observe $h \to b\bar{b}$ with S/B $\sim$ 1 in SUSY (mSUGRA), and Implications for Tracker and HCAL", *CMS-NOTE* **070** (1997).

[40] A. Datta, A. Djouadi, M. Guchait, and F. Moortgat, "Detection of MSSM higgs bosons from supersymmetric particle cascade decays at the LHC", *Nucl.Phys.* **B681** (2004) 31–64, `doi:10.1016/j.nuclphysb.2003.12.012`, `arXiv:hep-ph/0303095`.

[41] A. L. Read, "Presentation of search results: The CL_s technique", *J.Phys.* **G28** (2002) 2693–2704, `doi:10.1088/0954-3899/28/10/313`.

[42] A. L. Read, "Modified frequentist analysis of search results (The CL_s method)", *CERN-OPEN* **205** (2000).

[43] G. Cowan, K. Cranmer, E. Gross, and O. Vitells, "Asymptotic formulae for likelihood-based tests of new physics", *Eur.Phys.J.* **C71** (2011) 1554, `doi:10.1140/epjc/s10052-011-1554-0`, `arXiv:1007.1727`.

[44] ATLAS and CMS Collaboration, "Procedure for the LHC Higgs boson search combination in summer 2011",. ATL-PHYS-PUB-2011-11, CMS NOTE-2011/005.

[45] M. Botje et al., "The PDF4LHC working group interim recommendations", (2011). `arXiv:1101.0538`.

[46] CMS Collaboration, "CMS Luminosity Based on Pixel Cluster Counting - Summer 2013 Update", CMS Physics Analysis Summary CMS-PAS-LUM-13-001, CERN, (2013).